CHALMERS
UNIVERSITY OF TECHNOLOGY

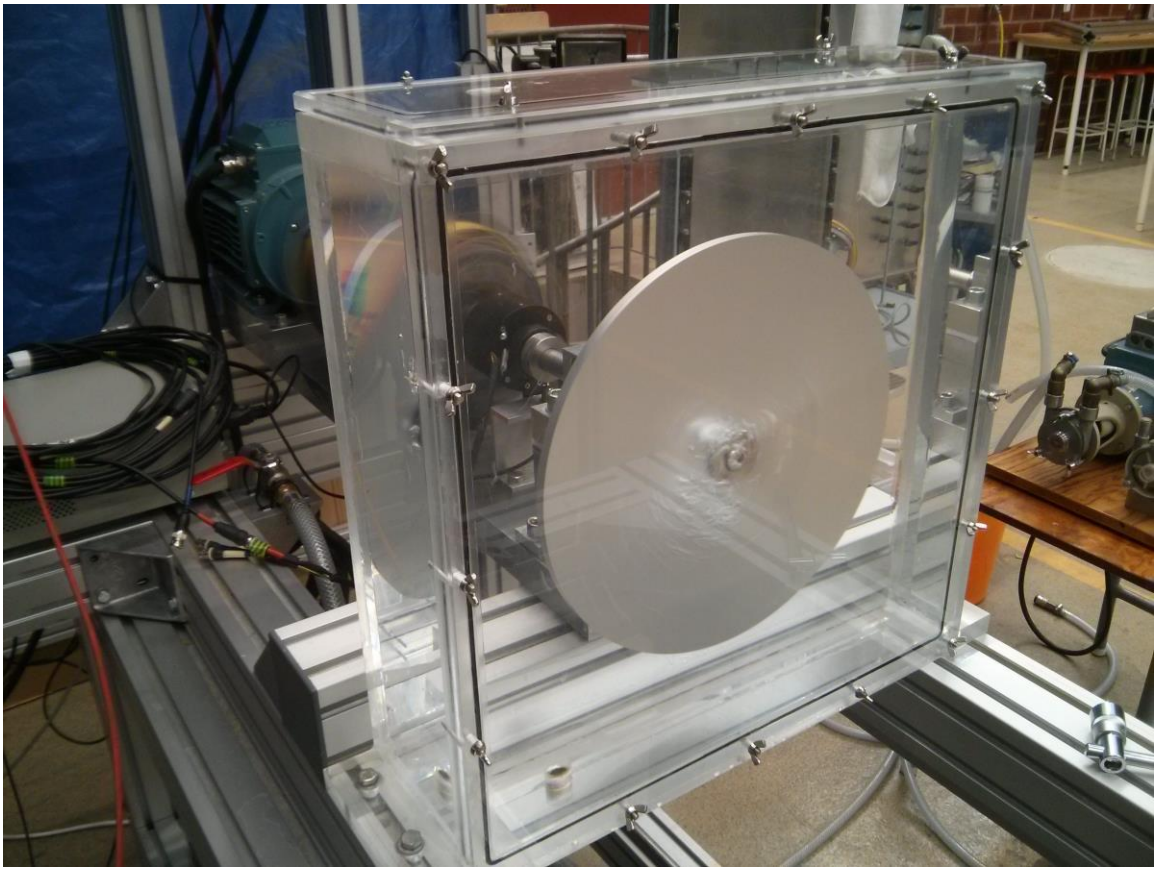

Turbulent boundary layer: comparison between a flat plate and a rotating disk with and without periodic roughness

Master's thesis in Applied Mechanics

José M Amor

Department of Applied Mechanics
CHALMERS UNIVERSITY OF TECHNOLOGY
Gothenburg, Sweden 2015

MASTER'S THESIS IN APPLIED MECHANICS

Turbulent boundary layer: comparison between a flat plate and a rotating disk with and without periodic roughness

José M Amor

Department of Applied Mechanics
Division of Fluid Dynamics
CHALMERS UNIVERSITY OF TECHNOLOGY
Göteborg, Sweden 2015

Turbulent boundary layer: comparison between a flat plate and a rotating disk with and without periodic roughness
José M Amor

Master's Thesis 2015:74
ISSN 1652-8557
Department of Applied Mechanics
Division of Fluid Dynamics
Chalmers University of Technology
SE-412 96 Göteborg
Sweden
Telephone: + 46 (0)31-772 1000

Department of Applied Mechanics
Göteborg, Sweden 2015-09-14

Turbulent boundary layer: comparison between a flat plate and a rotating disk with and without periodic roughness

Master's thesis in Applied Mechanics

José M Amor
Department of Applied Mechanics
Division of Fluid Dynamics
Chalmers University of Technology

ABSTRACT

In order to understand and predict the behavior of a flow around an object it is necessary to study the phenomenon present on the close-to-the-wall region of the flow, where the viscous forces cannot be neglected nor the variations of the properties of the flow. This region is called the *boundary layer*. In many situations, the contribution of the viscous friction in the boundary layer into the total drag can be substantial, and understanding of the effect of the roughness on the boundary layer is of importance. This project is focused on the study of the boundary layer created near two different objects: a flat plate and a rotating disk.

The flat plate is widely used in fundamental studies and in the engineering industry as an approximation of more complex models, for instance the ship hull in the naval engineering. The influence of the roughness on the friction drag can be obtained from testing of different plate models in a towing tank. Although this approximation usually offers a good agreement, experimental data and measurements are expensive to obtain. In order to reduce the cost of the experiments, a rotating disk is used an approximation of a flat plate since the installation and design of the experiment is not only cheaper but also simpler. The validation of this approximation is the main objective of this project and it is carried out by a study which is focused on finding similarities between both boundary layer properties with the aid of *Computational Fluid Dynamics (CFD)*. Also, experimental measurements are compared with CFD result with the aim of a validation of the CFD results.

Key words: boundary layer, computational fluid dynamics, rotating disk, flat plate, roughness, turbulence

Contents

Preface

In this study, computational results are obtained using a CFD software; Star-CCM+. In order to study the effects of the roughness, three rotating disks and three flat plates with different roughness are simulated. The rotating disks have been also used in an experiment for experimental data. The study has been carried out from February 2015 to July 2015. The work is a part of a research project concerning fluid properties over a ship hull. The project is carried out at the Department of Applied Mechanics, Fluid Dynamics, Chalmers University of Technology, Sweden.

This part of the project has been carried out with the PhD student Bercelay Niebles Atencio and the associate professor Valery Chernoray as supervisors. All the simulations have been carried out in the computer's room at the Department of Applied mechanics, as well as the experiments in the laboratory. I would like to thank Borja Rojo and Meisam Farzaneh for their help and advice throughout this project

Finally, it should be noted that the tests could never have been conducted without the sense of high quality and professionalism of the department staff.

Göteborg June 2015

José M Amor

Notations

These are all the variables that appear inside the report and their meanings.

$\boldsymbol{\rho}$	Density
$\boldsymbol{t}$	Time
$\boldsymbol{u, v, w}$	Components of velocity of a fluids particle
$\boldsymbol{\nu}$	Kinematic viscosity
$\boldsymbol{E_p}$	Modulus of elasticity
μ	Dynamic viscosity
$\boldsymbol{E}$	Energy
$\boldsymbol{\tau}$	Wall shear stress
u_τ	Friction velocity or shear velocity
$\boldsymbol{\delta}$	Boundary layer thickness
$\boldsymbol{U_\infty}$	Free stream velocity
$\boldsymbol{Re}$	Reynolds number
$\boldsymbol{\varepsilon}$	Dissipation of turbulent kinetic energy
$\boldsymbol{u_k}$	Root mean square of the velocity
$\boldsymbol{\eta}$	Kolmogorov length scale
$\boldsymbol{\tau_\eta}$	Kolmogorov time scale
$\boldsymbol{u_\eta}$	Kolmogorov velocity scale
$\boldsymbol{\bar{u}}$	Time averaged velocity
$\boldsymbol{u_i', u_j', u_k'}$	Components of the fluctuating velocity
$\boldsymbol{\bar{u}'}$	Mean of the fluctuating velocities
$\boldsymbol{f_i}$	Vector of external forces
$\boldsymbol{k}$	Turbulent kinetic energy
μ_t	**Eddy viscosity**

1 Chapter I: Introduction

The study of fluid dynamics is one of the branches inside the applied mechanics field. Its aim is to understand and comprehend what happens to a fluid when it travels around a body. When a free stream flow encounters an object on its path, as the fluid cannot go through it, the flow is deviated changing not only its direction but also some of its properties in the zones close to the object. Here is where the fluid dynamics study appears. One of its most important applications among others is engineering, since most of the moving objects are surrounded by fluids (air, water…). The closer we are to understand the phenomenon that appears around the objects, the easier it is to obtain the desires properties.

According to what was previously mentioned, assuming that the fluid properties change when it encounters something on its path, one could intuit that these properties will change depending on the characteristics of the object itself (shape, temperature…). This project will be focused on understanding what happens to the fluid when it travels around two specific geometries and with certain conditions or assumptions, making it easier to comprehend it in a micro-scale size.

Modern fluid dynamics are based on the Claude-Louis Henri Navier and George Gabriel Stokes' work. Their work led to a group of non-linear partial differential equations, which come from applying Newton's second law to a fluid motion in 3D and they explain the fluids behavior taking into account all internal and external forces and they are known as the Navier-Stokes equations (N-S equations):

$$Continuity: \frac{\partial \rho}{\partial t} + \frac{\partial(\rho u)}{\partial x} + \frac{\partial(\rho v)}{\partial y} + \frac{\partial(\rho w)}{\partial z} = 0 \tag{1}$$

$$X - Mom: \frac{\partial(\rho u)}{\partial t} + \frac{\partial(\rho u^2)}{\partial x} + \frac{\partial(\rho uv)}{\partial y} + \frac{\partial(\rho uw)}{\partial z} = -\frac{\partial p}{\partial x} + \nu\left(\frac{\partial^2 u}{\partial x^2} + \frac{\partial^2 u}{\partial y^2} + \frac{\partial^2 u}{\partial z^2}\right) \tag{2}$$

$$Y - Mom: \frac{\partial(\rho v)}{\partial t} + \frac{\partial(\rho uv)}{\partial x} + \frac{\partial(\rho v^2)}{\partial y} + \frac{\partial(\rho vw)}{\partial z} = -\frac{\partial p}{\partial y} + \nu\left(\frac{\partial^2 v}{\partial x^2} + \frac{\partial^2 v}{\partial y^2} + \frac{\partial^2 v}{\partial z^2}\right) \tag{3}$$

$$Z - Mom: \frac{\partial(\rho w)}{\partial t} + \frac{\partial(\rho uw)}{\partial x} + \frac{\partial(\rho vw)}{\partial y} + \frac{\partial(\rho w^2)}{\partial z} = -\frac{\partial p}{\partial z} + \nu\left(\frac{\partial^2 w}{\partial x^2} + \frac{\partial^2 w}{\partial y^2} + \frac{\partial^2 w}{\partial z^2}\right) \tag{4}$$

$$Energy: \frac{\partial(\rho E)}{\partial t} + \frac{\partial(\rho uE)}{\partial x} + \frac{\partial(\rho vE)}{\partial y} + \frac{\partial(\rho wE)}{\partial z} = -\frac{\partial(pu)}{\partial x} - \frac{\partial(pv)}{\partial y} - \frac{\partial(pw)}{\partial z} + S \tag{5}$$

However, this is not applicable to all the known fluids, but just the Newtonian ones. A fluid is Newtonian if its viscous stress is linearly proportional to the local strain rate or, to put it in another way, the viscous force is proportional to the changes of the velocity vectors along the object:

$$\tau = \mu \frac{\partial u}{\partial y} \tag{6}$$

In the case of study, the fluid is water, which is a Newtonian fluid, making the N-S equations applicable to this case.
Resolving these equations is very complex and it should be done for every particle in the flow, making it impossible to achieve. Due to big improvements on computational resources for the last years, it is possible to obtain close approximations to the N-S equations for some cases with Computational Fluid Dynamics programs (CFD). These programs work with discretized volumes (meshes) and, using algorithms based on iterations, they calculate an approximate solution of the set of equations for each cell in the mesh. Throughout this project, it will be explained how these programs work and which are the best ways to discretize and model different cases, as well as their procedures to resolve them.
As mentioned before, it is considered of high interest to study the developed flow around two different geometries, and those are: a flat plate and a rotating disk. The main objective of the project is to understand the phenomena that occur in the flow near the wall of a flat plate with the aid of simulating and experimental data. Simulated data can be obtained through CFD programs, sometimes with a very high computational cost when the resolution methods demand a very refined mesh. Experimental data can also be hard to get due to money, time and space cost of the mounting. If one wants to measure flow properties near a flat plate, the plate should be placed inside a pipe with a diameter big enough so that the phenomena near the pipe wall does not interfere with the phenomena near the plate. The pipe should lead the flow in a closed circuit so the plate is fully emerged inside the same flow, connecting the outlet of the flow (right after the flat plate) with the inlet (in the leading edge of the plate). In order to achieve that, it is required a bomb to impulse all the flow throughout the circuit. It is clear then, that the bigger the plate is, the bigger the full mounting will be, making it very expensive and hard to build. Here is where the rotating disk becomes important since the assembly and mounting of a rotating disk experiment can be simpler and cheaper. Fewer elements with simpler geometries are needed such as a square box tank, a disk, a motor (which makes the disk rotate) and a shaft that connects the disk with the motor. Once it is understood that the rotating disk experiment is more viable than the flat plate experiment, if a relation between both phenomena is found, it would be possible to obtain the desired experimental data of a plate with a lower cost and time.

Despite the fact that a few studies focused on rotating disk and flat plates have been carried out already, more information is necessary in order to understand the similarities between the boundary layers on both cases.

2 Chapter II: Theory concepts

In order to get a better understanding of the physics that are relevant to this project, a few theory concepts will be explained below.

2.1 Fluid motion

In the theoretical investigations inside the fluid dynamics field, it is usually considered a perfect fluid, which means it is frictionless and incompressible. If you model the fluid as a union of different and parallel layers, during the motion of the fluid these layers will not apply any shear stress between them, and only pressure forces will appear (normal direction of the layers). According to this assumption, no object would suffer from any tangential or friction force, which leads to the statement that an object would suffer no drag when surrounded by a flow in motion called d'Alember's Paradox [1].
Therefore there exists a shear stress between the layers of a flow (asides from the pressure forces) near the wetted wall of a solid which explains the drag effect. These friction or tangential forces are the result of a fluid property called viscosity.

2.2 Viscosity

The concept of viscosity is easier to understand by visualizing it with an example. Consider the motion of a fluid between two flat plates separated at a distance noted as *h*. One of them is fixed, while the other one is moving with a defined velocity *U*. See figure 1:

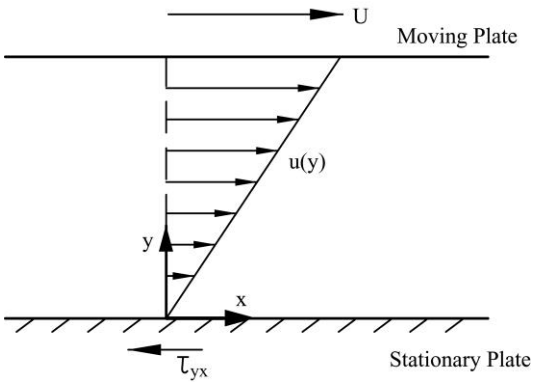

Fig 1. Velocity distribution between two flat plates, from [2]

The experiments have shown that the fluid adheres to the body's surfaces, fixing the velocities of the flow touching the plates. The velocity of the flow touching the bottom is zero, since the plate is not moving while the top velocity is *U*. There exists then a linear velocity distribution which increases as the fluid is close to the moving wall:

$$U(y) = \frac{y}{h}U \tag{7}$$

It can be seen that for *y=0*, the velocity is zero and for *y=h* the velocity is *U* which corresponds with what was mentioned below.
In order to achieve the motion, it is necessary a transmission of tangential forces between each layer, starting with the one touching the wall, so that each subsequent layer is dragged forwards causing the flow to move. With the aid of experiments, it is known that this force is proportional to the velocity of the moving plate *U* and inversely proportional to the separation of the plates *h*. Hence it can be obtained the expression of the frictional shear stress per unit area τ, as shown below:

$$\tau = \mu \frac{\partial u}{\partial y} \tag{8}$$

where μ (dynamic viscosity) is the proportionality factor between the frictional shear stress and the gradient of the velocity profile along the gap between the plates. It is important to note that, in fluid motions where inertia and frictional forces interact, a parameter called *kinematic viscosity* (ν) will be meaningful:

$$\nu = \frac{\mu}{\rho}, \quad \text{where } \rho \text{ denotes density.} \tag{9}$$

2.3 Incompressibility

The compressibility (or incompressibility in our case) of a fluid is the measure of the volume change of a gas or liquid due to the action of external forces. It can be defined then a *modulus of elasticity* E_p that connects both terms:

$$\Delta p = -E_p \frac{\Delta V}{V_0} \tag{10}$$

In this equation, it is shown the relation between the change of volume ($\Delta V/V_0$) and the pressure variation (Δp).
Owing to the mass conservation inside a control volume, the equation can be written with density terms instead of volume terms, leading to the following expression:

$$\Delta p = E \frac{\Delta \rho}{\rho_0} \tag{11}$$

In order to classify a flow as incompressible, it is necessary that the change of volume or density must be very small, consequently:

$$\frac{\Delta \rho}{\rho_0} \ll 1 \tag{12}$$

In both of our cases, the flow involving the study will be considered as an incompressible flow.

2.4 Similar flows and Reynolds number

In order to consider similar two flows that go throughout geometrically similar bodies with different velocities, dimensions and different fluid, one condition must be satisfied: the forces applied on every point of the body from every particle in the surrounding fluid must have fixed ratio for every instant of time.
One shall consider now the case when only inertial and frictional forces are present. Other forces such as elastic forces, which may come from changes of volume, won't be considered since the flow being studied is incompressible. Gravitational forces inside the fluid are compensated by buoyancy so they can be excluded as well. Once these assumptions are accepted, the condition of similarity is only satisfied if the ratio between the inertial forces and the friction forces are the same for every corresponding point. This ratio is known as the Reynolds number. The following equation corresponds to the lineal Reynolds number:

$$Re = \frac{inertial\ forces}{friction\ forces} = \frac{\rho\, V\, d}{\mu} = \frac{V\, d}{\nu} \tag{13}$$

Here V denotes the velocity of the free stream's flow, *d* denotes the characteristic length of the object and ν, as mentioned above, it's the kinematic viscosity. In the case of a flat plate, the characteristic length is the longitude of the plate in the direction of the flow, whereas in the rotating disk, the characteristic length is the radius of the disk.

Then the flow is rotational and not lineal for instance in a rotating disk, the equation of the Reynolds number changes, leading to the following formula:

$$Re = \frac{r\sqrt{\omega_{rot}}}{\sqrt{\nu}} \tag{14}$$

Being ω_{rot} the rotational speed in rad/s.

2.5 Boundary-layer

In cases of fluids in motion at high Reynolds numbers, where the perfect fluid theory is applicable due to the pressure distribution, the viscous effects are only considerable inside a thin layer near the wetted wall of the solid. However, in the case of a real fluid, it is necessary that the non-slip condition near the wall is satisfied, otherwise there would not be an appreciable difference compared to the case of a perfect fluid. The non-slip condition refers to the fact that the fluid adheres to the wall, causing the flow to be retarded due to frictional forces

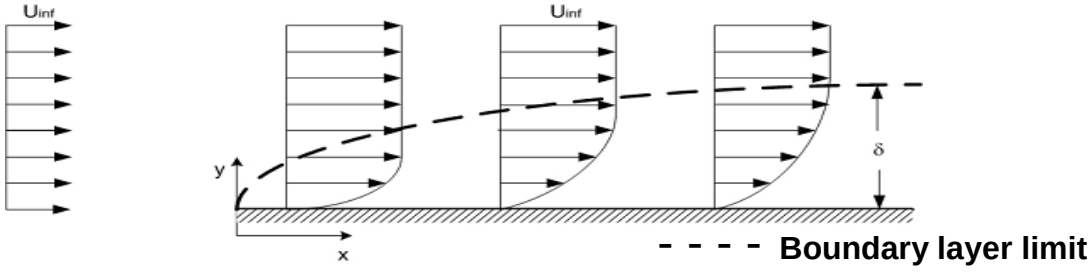

Fig 2. Velocity profile of the flow around a flat plate, from [3]

between the layers. However, this effect decreases as the distance from the wall increases, reaching one point where the viscous forces are negligible and, consequently, the velocity profile becomes constant with the same value as the free stream. This group of layers where the viscous forces need to be taken into account is called the *boundary layer*, and this concept was mentioned for the first time by L. Prandtl in a flat plate case.

It is seen in the figure 2 that the velocity of the fluid is considerably lower in the proximities of the wall than in a big distance from it. The thickness of the boundary layer increases with the throughout the flat plate in the downstream direction. It can be noticed that the thickness of the layer δ increases continuously in the downstream direction. As it can be deduced, the thickness also increases as the viscosity increases.
Even with small viscosities (high Reynolds numbers) the frictional shear stress $\tau=\partial u/\partial y$ is still considerable inside the boundary layer, since the gradient of velocities across the flow is large in it. However, as it is already seen, this gradient is very small outside the boundary layer where the frictional shear stress is negligible. It is then recommended to divide the case in two different regions in order to ease the mathematical analysis: the region inside the boundary layer where the frictional forces due to viscosity must be taken into account, and the region outside the boundary layer, where these forces can be neglected and then the perfect fluid theory is applied, what gives acceptable results with an easier analysis.

The behavior of the flow surrounding the second object of study (rotating disk) differs from the behavior over a flat plate. First of all, a three-dimensional analysis is needed and it cannot be simplified as a two-dimensional analysis as with a flat plate. Since the velocity field has three components, three different boundary layers are generated around the disk. A graphic explanation is shown further.

2.5.1 Boundary layer over a flat plate

We shall now consider the simplest case, the boundary layer generated over a flat plate. First of all, a coordinate system must be specified. The leading edge of the flat plate will be set at $x = 0$, the x-axis will go along the plate in the downstream direction as shown in the figure 3.

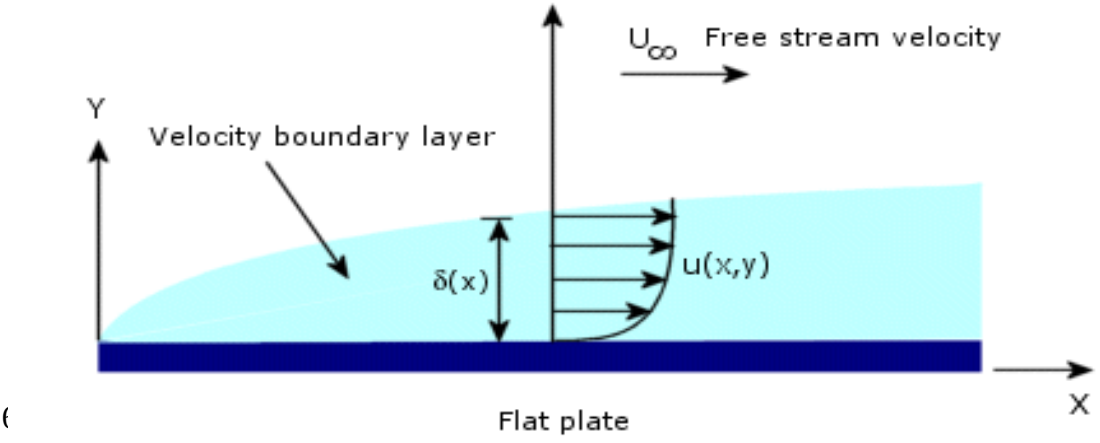

Fig 3. Velocity profile inside a boundary layer, from [4]

The flow considered has a free stream velocity (U_∞) profile parallel to the flat plate. Since this is a simplified two-dimensional case, the equations governing the boundary layer and the boundary conditions become:

$$\frac{\partial u}{\partial x} + \frac{\partial v}{\partial y} = 0 \tag{15}$$

$$u\frac{\partial u}{\partial x} + v\frac{\partial v}{\partial y} = \nu\frac{\partial^2 u}{\partial y^2} \tag{16}$$

$$y = 0: \quad u = v = 0 \tag{17}$$

$$y = \infty: \quad u = U_\infty \tag{18}$$

Since no length is fixed in the system, it is acceptable to presume that the velocity profiles $u(y)$ at different x values should be similar to each other. In order to make them identical, it is necessary to transform the variables u and y with scale factors being those the velocity of the free stream U_∞, and the boundary layer thickness $\delta(x)$. As it has been explained before, the thickness of the boundary layer increases as the x value increases, so we need to calculate the thickness before we can transform the variables.
If we consider the boundary layer thickness as the distance from the wall where the velocity is approximately 99% of the free stream velocity i.e. $u = 0.99U_\infty$, it is possible to plot the different velocity profiles along the flat plate as one single curve with the scaling factors, leading to a graph similar to the one in figure 4.

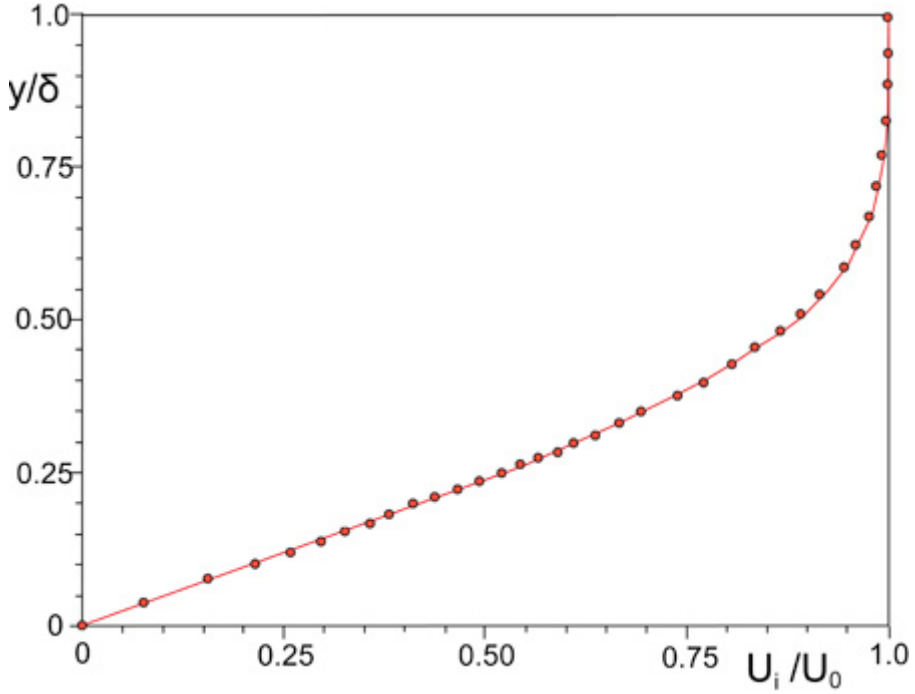

Fig 4. Example of a dimensionless plot of distance from the wall - velocity

However, the profile obtained on the figure 4 depends on the external conditions and the properties of the fluid, i.e. the Reynolds number. As the Reynolds number changes, the profile also changes with it.

At low Re the flow is considered $laminar$, as it increases the $transition$ occurs and if the Re is large enough ($3.5 \cdot 10^5 - 10^6$) the flow becomes $turbulent$.

2.5.2 Couette flow

The flow motion between two parallel smooth surfaces (one moving and the other one stationary), expecting a Couette flow.

A Couette flow [5] is the one generated between two parallel flat plates, when one of them is moving dragging the flow while the other one is fixed and this flow is laminar. This is the theoretical velocity profile of a Couette flow (Figure 5):

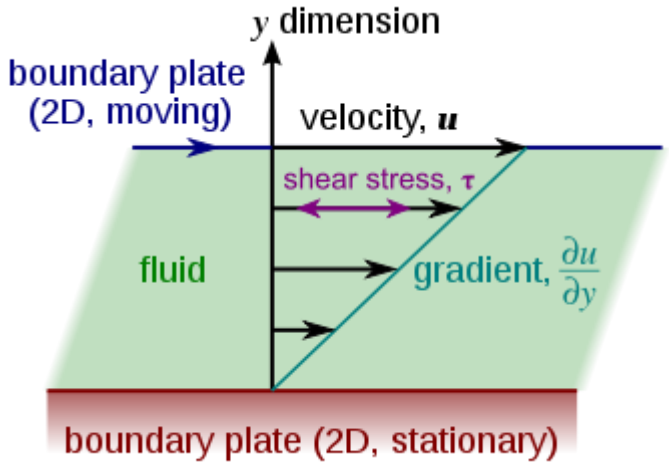

Fig 5. Couette velocity profile, from [6]

2.5.3 Boundary layer over a rotating disk

The motion of the fluid around a rotating disk cannot be simplified as a two dimensional case as it is done with the flat plate. The rotating disk flow has three different components of velocity: axial, radial and tangential, shown in figure 6.

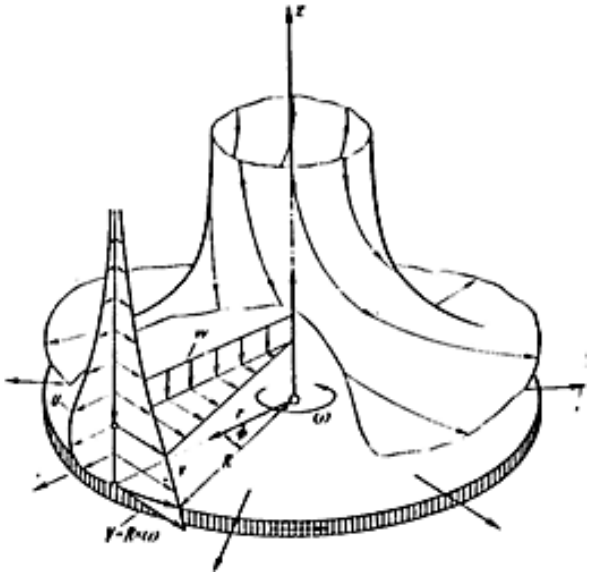

Fig 6. Flow motion over a rotating disk, from [7]

The axial component is by the order of magnitude smaller than the radial and tangential components. Furthermore, the variation of the velocity and pressure in the axial direction near the disk is much larger than the rate of their variation in the radial direction. Therefore, the tangential velocity component is the dominant component. In such cases, since the disk is fully immersed in water and the flow around the disk is uniform, only a slice of the disk can be modeled (figure below).
For such modeling, the following assumptions are made:

- Steady state flow
- Periodic boundary conditions

2.5.4 Laminar to turbulent: transition

When a flow is considered under laminar regime, the velocity profile is "stable", which means that the velocity vector defined by every particle inside the boundary layer is uniform and parallel to the plate. However, at high Reynolds numbers the particles start mixing due to the effect of the superimposition of different motions inside the flow. The first motion leads the flow downstream in the direction of the axis, while the second motion creates fluctuations between the particles, making the flow to diffuse into the stream. These fluctuations have their origin in the exchange of momentum in transversal directions because each particle holds its forward momentum during the mixing. As a result, a more uniform velocity distribution in the cross-section is obtained, compared to the one obtained in a laminar flow.
On closer investigations, it was seen that the essential effect of turbulence is the fact that the velocity and pressure given at one point are not constant through

time but have non-regular fluctuations at high frequencies. Since the velocity of every point is not constant, its velocity is considered as the average of the different velocities of the same point over time.

It is proven, through many experiments, that flows with Reynolds numbers below 2000 remain laminar [8], even with the presence of strong disturbances. However, there is not an exact Reynolds number where the flow strictly loses its laminar behavior, since it depends on the conditions of the flow before it contacts the plate.
Detailed investigations have shown that between the laminar regime and the turbulent regime, there is a range of Reynolds number where the flow becomes intermittent, switching alternatively its behavior from laminar to turbulent over time. The figure 7 shows both regimes (laminar and turbulent) and the region in between (transition).

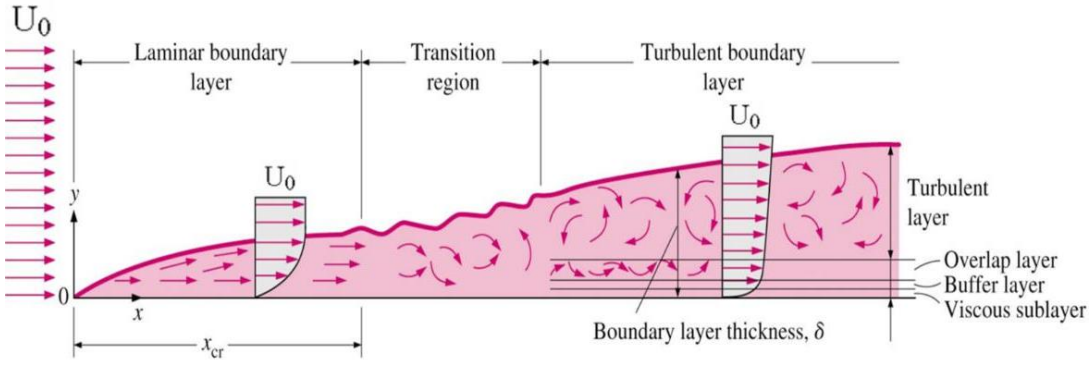

Fig 7. Regions of a boundary layer: laminar, transition and turbulent, from [9]

2.5.5 Turbulence

In the laminar regime of a boundary layer, all the perturbations are absorbed by the viscous forces, predominant on the laminar regime. As the Reynolds number increase, the inertial forces grow and they become more dominant compared to the viscous forces. There is a point, where the previously mentioned perturbations are so intense, that they cannot be absorbed by the viscous forces, destabilizing the flow. At this point, it is considered that the transition region begins. As the Reynolds number is increased, the boundary layer turns to a fully turbulent layer, where the characteristics properties are: low momentum diffusion, fast variation of velocity and pressure in space and time, and high momentum convection.

2.5.6 Eddies

A flow is considered turbulent when its motion has irregular fluctuations (due to mixing or eddies) superimposed to the main stream. However, the lumps that perform the fluctuations should not be considered as single molecules but small balls with varying size called eddies.

2.5.7 Law of the wall: logarithmic law

One of the objects of study in this project is the similarity between the logarithmic laws of the two different boundary layers. In fluid dynamics, the law of the wall, mentioned for the first time by Theodore von Kármán [9] says that at certain point, the averaged values of the velocities are proportional to the logarithmic value of the distance from the wall to that point.

$$U^+ = \frac{1}{k}\, ln\, Y^+ + C^+ \tag{19}$$

Both U^+ and Y^+ are dimensionless values. The definition of these parameters are:

$$Y^+ = \frac{y\, u_\tau}{\upsilon} \tag{20}$$

$$U^+ = \frac{u}{u_\tau} \tag{21}$$

$$u_\tau = \sqrt{\frac{\tau}{\rho}} \tag{22}$$

Where τ is the wall shear stress and u_τ is the friction velocity or the shear velocity.
The experimental values of the parameters k and C^+ are 0.41 and 5.0 respectively for a smooth surface.

2.6 Computational fluid dynamics: resolution methods

Two different resolution methods were considered initially for the simulations that were going to be carried out. Inside this chapter, a brief explanation of each method is done and the reasons why each method has been discarded have been explained.

2.6.1 Direct numerical simulation

The first model that was considered is the Direct Numerical Simulation, also known as DNS. In this simulation, the Navier-Stokes equations are solved without using any turbulence model, meaning that both the time scales and the spatial case must be resolved without using any model. This means that even the smallest scales must be resolved inside the computational mesh. In order to determine the smallest scale where there is a dissipation of energy and consequently the cell size, a new term is defined: the Kolmogorov microscales.

2.6.1.1 Kolmogorov microscales

The smallest scales inside a turbulent flow are called the Kolmogorov microscales (Kolmogorov's theory, 1941). When a region is inside the Kolmogorov microscales, it means that the viscosity is dominant, making the turbulent kinetic energy dissipate into heat. Before explaining the three

Kolmogorov microscales, it is necessary to introduce a new parameter: the dissipation of turbulent kinetic energy (ε).

$$\varepsilon = \frac{{u_k}^3}{L} \tag{23}$$

where u_k is the root mean square of the velocity.

Once the ε is defined it is possible to see the three different Kolmogorov microscales:

Kolmogorov length scale	Kolmogorov time scale	Kolmogorov velocity scale
$\eta = \left(\frac{\nu^3}{\varepsilon}\right)^{1/4}$	$\tau_\eta = \left(\frac{\nu}{\varepsilon}\right)^{1/2}$	$u_\eta = (\nu\varepsilon)^{1/4}$

Tab 1. Kolmogorov scales

where ν is the fluid's kinematic viscosity and ε is the average rate of the dissipation of the turbulent kinetic energy per unit mass.

As it can be seen in the formulas, these scales depend only on ν and ε and they are independent of the mean flow field and the boundary conditions. In Andrey Kolmogorov's theory it is explained how the energy is transferred from the bigger eddies to the smaller eddies, how much energy an eddy has (given its size) and how much energy is dissipated on each eddy. He also stated that the smallest scales of turbulence are the same for every turbulent flow and they can be deduced by a dimensional analysis.

The Direct Numerical Simulation is the most accurate numerical technique since it resolves the fluid in all scales, so it provides the exact results. However, this model is not used very often due to a very high computational cost, which will be explained later in this report.

2.6.2 Large Eddy Simulation (LES)

Large eddy simulation (LES) is a popular technique for simulating turbulent flows. An implication of Kolmogorov's theory of self similarity is that the large eddies of the flow are dependent on the geometry while the smaller scales more universal. This feature allows one to explicitly solve for the large eddies in a calculation and implicitly account for the small eddies by using a subgrid-scale model (SGS model) [11].
This method has a considerable computational cost (lower than the DNS). For that reason, a CFD model was used in order to reduce the cost due to physical and time resource limitations.

2.7 CFD model: Reynolds Averaged Navier-Stokes (RANS)

The Reynolds Averaged Navier-Stokes equations of a fluid flow motion are time averaged approximations of the Navier-Stokes equations. This idea comes from the Reynolds decomposition [12], where the instantaneous properties of the flow are decomposed into a mean component and a fluctuating component. Here is an example of the velocity decomposition:

$$u = \bar{u} + u' \tag{24}$$

where u is the instantaneous velocity, $\bar{u}$ is the time averaged velocity and u' is the fluctuating velocity. One of the properties of this decomposition is that the mean of the fluctuating velocities equals to zero, i.e. $\overline{u'} = 0$. With the aid of this decomposition, the incompressible Navier-Stokes equations can be transformed in the following time-averaged equations, being $\overline{f_i}$ the vector of external forces:

$$\frac{\partial \bar{u}_i}{\partial x_i} = 0 \tag{25}$$

$$\frac{\partial \bar{u}_i}{\partial t} + \bar{u}_j \frac{\partial \bar{u}_i}{\partial x_j} + \overline{u'_j \frac{\partial u'_i}{\partial x_j}} = \overline{f_i} - \frac{1}{\rho}\frac{\partial \bar{p}}{\partial x_i} + \nu \frac{\partial^2 \bar{u}_i}{\partial x_j \partial x_j} \tag{26}$$

Throughout this section, we will focus in two two-equation linear eddy viscosity models: the k-epsilon model and the k-omega model.
These are the most common types of turbulence modelling in the engineering industry, and they are still under investigation in order to obtain more refined and accurate models.

They are called two-equation models due to the fact that they include two extra equations that represent the transport of the turbulent properties in the flow. This is helpful in order to calculate effects such as convection and the diffusion of turbulent energy. As it is just mentioned, these models represent the transport of turbulent properties. One of the properties is the turbulent kinetic energy, also noted as k, while the second property may vary depending on the model used. The turbulent kinetic energy is defined as the mean kinetic energy per mass volume that is related with the eddies in a turbulent flow.

$$k = \frac{1}{2}\left(u'^2_i + u'^2_j + u'^2_k\right) \tag{27}$$

One of the assumptions on both k-epsilon and k-omega models is that the velocity fluctuations are isotropic, which means:

$$u'^2_i = u'^2_j = u'^2_k \tag{28}$$

If we combine equation 27 and equation 28, the value of k can be calculated as:

$$k = \frac{3}{2}u'^2_i \tag{29}$$

2.7.1 K-Epsilon standard turbulence model

The most common turbulent model for the past years is the $k-\varepsilon$ model (Jones & Launder, 1972) which has, in addition to the k equation, an extra equation based on the dissipation of the turbulent kinetic energy (ε). The transport equations added to the RANS equations are:

- For turbulent kinetic energy:

$$\frac{\partial(\rho k)}{\partial t}+\frac{\partial(\rho k u_i)}{\partial x_i}=\frac{\partial}{\partial x_j}\left[\frac{\mu_t}{\sigma_k}\frac{\partial k}{\partial x_j}\right]+2\mu_t E_{ij}E_{ij}-\rho\varepsilon \tag{30}$$

- For dissipation:

$$\frac{\partial(\rho \varepsilon)}{\partial t}+\frac{\partial(\rho \varepsilon u_i)}{\partial x_i}=\frac{\partial}{\partial x_j}\left[\frac{\mu_t}{\sigma_\varepsilon}\frac{\partial \varepsilon}{\partial x_j}\right]+C_{1\varepsilon}\frac{\varepsilon}{k}2\mu_t E_{ij}E_{ij}-C_{2\varepsilon}\rho\frac{\varepsilon^2}{k} \tag{31}$$

Where u_i represents the velocity component on the i direction , E_{ij} represents the component of rate of deformation and μ_t represents the eddy viscosity defined as:

$$\mu_t=\rho C_\mu\frac{k^2}{\varepsilon} \tag{32}$$

These equations also have some constants, which value is obtained using a curve fitting for a large range of experimental data for turbulent flows [13]:

C_μ	σ_k	σ_ε	$C_{1\varepsilon}$	$C_{2\varepsilon}$
0.09	1.00	1.30	1.44	1.92

The k-ε model has been designed for planar shear layers and recirculating flows. It is usually useful for free-shear layer flows with small adverse pressure gradients. It can also be stated as the simplest turbulence model for which it's only needed to define initial and/or boundary conditions. The advantages of this model, among others, are robustness, easy implementation and low computational cost. However, it only works for turbulent flows and does not perform well with strong curvature on the streamlines and rotating flows.

2.7.2 K-Omega standard turbulence model

The other model worth to mention in this section is the $k-\omega$ model. The physical meaning of the k is the same as in the $k-\varepsilon$ model, but here the second parameter which defines the transport of turbulence is the specific ratio of dissipation of turbulent kinetic energy, also known as ω.

The standard $k-\omega$ model was formulated by Wilcox [14]. The evolution of k and ω is modeled as:

$$\frac{\partial(\rho k)}{\partial t}+\frac{\partial(\rho k u_j)}{\partial x_j}=P-\beta^*\rho\omega k+\frac{\partial}{\partial x_j}\left[\left(\mu+\sigma_k\frac{\rho k}{\omega}\right)\frac{\partial k}{\partial x_j}\right],\quad with\ P=\tau_{ij}\frac{\partial u_i}{\partial x_j} \tag{33}$$

$$\frac{\partial(\rho\omega)}{\partial t}+\frac{\partial\left(\rho\omega u_j\right)}{\partial x_j}=\frac{\omega\gamma}{k}P-\beta\rho\omega^2+\frac{\partial}{\partial x_j}\left[\left(\mu+\sigma_k\frac{\rho k}{\omega}\right)\frac{\partial\omega}{\partial x_j}\right]+\frac{\sigma_d\rho}{\omega}\frac{\partial k}{\partial x_j}\frac{\partial\omega}{\partial x_j} \tag{34}$$

In comparison with the $k-\varepsilon$ model, this model performs better near the wall, it can handle the laminar-turbulent transition (usually predicting a bit earlier) and it also supports low Reynolds number flows. Nevertheless, this model is very sensible to turbulence on the inlet and the free stream, and also requires a refined mesh near the wall in order to resolve the viscous sub-layer.

2.7.3 Shear stress transport (SST) k-omega turbulence model

This is the model used in the simulations. The SST $k-\omega$ turbulence model designed by Menter [15,16], combines the advantages from both $k-\varepsilon$ and $k-\omega$ models. When close to the wall, it uses the $k-\omega$ formulation in order to resolve the viscous sub-layer and the inner parts of the boundary layer. However, the SST formulation switches to the $k-\varepsilon$ model on the free stream region, minimizing the sensitivity of the model against external turbulences in the inlet. Since the sub-layer is resolved, this model also requires a high-resolution mesh near the wall.

3 Chapter III: Methodology

Thanks to the technological researches carried out for the past decades, now it is possible to find solutions and predict the fluids behavior as well as the forces that affect the bodies surrounded by the fluid by using computational resources. Throughout this chapter, the methodology used in order to do the simulations which bring these solutions is explained starting from the creation of the geometry, followed by the discretization of the volume using a mesh and the resolution of the simulation using a computational fluid dynamics software.

3.1 Geometries

The creation of two different geometries has been done using a CAD software program called SolidWorks, being those a flat plate and a disk. Since the region studied is not the solid itself but the fluid domain which is in contact with the solid, the geometry is a fluid volume where the characteristics of the flow will be studied.

Choosing a good geometry is essential. Designing a proper geometry eases the creation of a high quality mesh (explained in the next section *Spatial discretization: Mesh*). One of the parameters that must be taken into account is the size of the geometry, which is strongly linked to the number of elements of the mesh and therefore, to the computational cost of the simulations. As reducing the computational cost has been considered of utmost importance, special geometries have been created for the simulations (different geometries from a flat plate and a disk). Instead of creating a geometry containing the whole control volume over the flat plate and the disk, a differential domain of the flow path has been created, reducing drastically the dimensions of the volume studied and therefore the computational cost of the simulations. However, this simplification requires a few specific boundary conditions which are explained further.

The geometry in the figure 8 can be considered as a scaled model of a normal sized flat plate, which would give good results by simply setting up a similar Reynolds number between the normal model and the scaled model. For simplicity, a two-dimensional model has been used, considering that the transversal component of the velocity is zero. The dimensions of the flat plate domain are 35 mm length and 50 mm high. It should be noted that the boundary layer generated over a flat plate is different from the boundary layer of the case of study. There are two main differences:

- Usually, a flat plate has a defined length, while the case of study is based on a plate with an infinite length.
- In this case, the flow travels between two flat plates (Couette flow) and it differs from the common case of a flow traveling over a single flat plate.

For these reasons, the first case of study (flat plate) is not strictly a boundary layer over a flat plate, but it has been named this way because the flow goes in one direction parallel to the surfaces and the emphasis is on the bottom plate

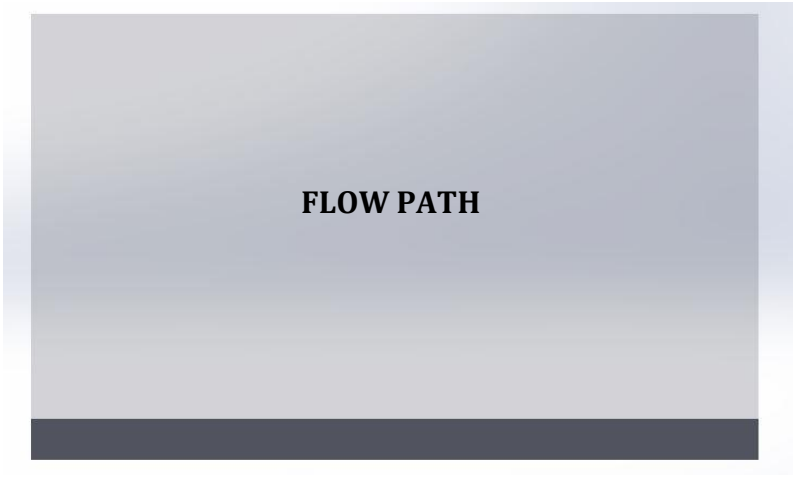

Fig 8. 2D flat plate and flow path

flow.

As seen in the following figure (Fig 9) only a partial volume of the full disk has been simulated. It is assumed that by setting up the proper periodic conditions the results are the same as if the full disk was simulated but with a considerable lower number of elements and therefore the computational cost.
The dimensions of the partial domain are: internal radius of 148 mm, external radius of 150mm, height of 50 mm (the same as the flat plate) and an angle of 0.233 rad.

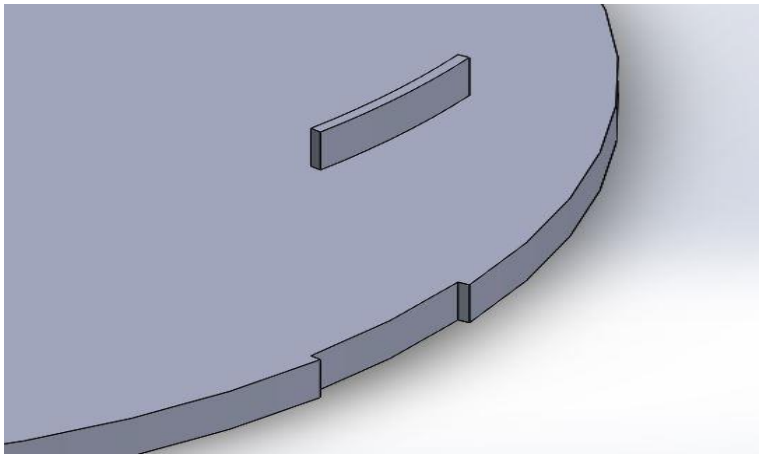

Fig 9. Differential domain of the smooth disk

The two geometries are not identical since the disk has a curvature that the flat plate does not have. However, the similarities between both geometries are believed to be good enough so the cases can be compared by setting up the correct boundary conditions.

Also two additional geometries are created which represent the two different artificial roughness. The design of this particular shape of roughness comes from the experiments that have been carried out during this project. Since both

simulated cases (flat plate and rotating disk) have been compared between them and the results from the simulated rotating disk have been compared with the measurements from an experimental rotating disk, the roughness had to be almost identical to the disk from the experiment. The experimental disk has this artificial roughness shown below (Figure 10):

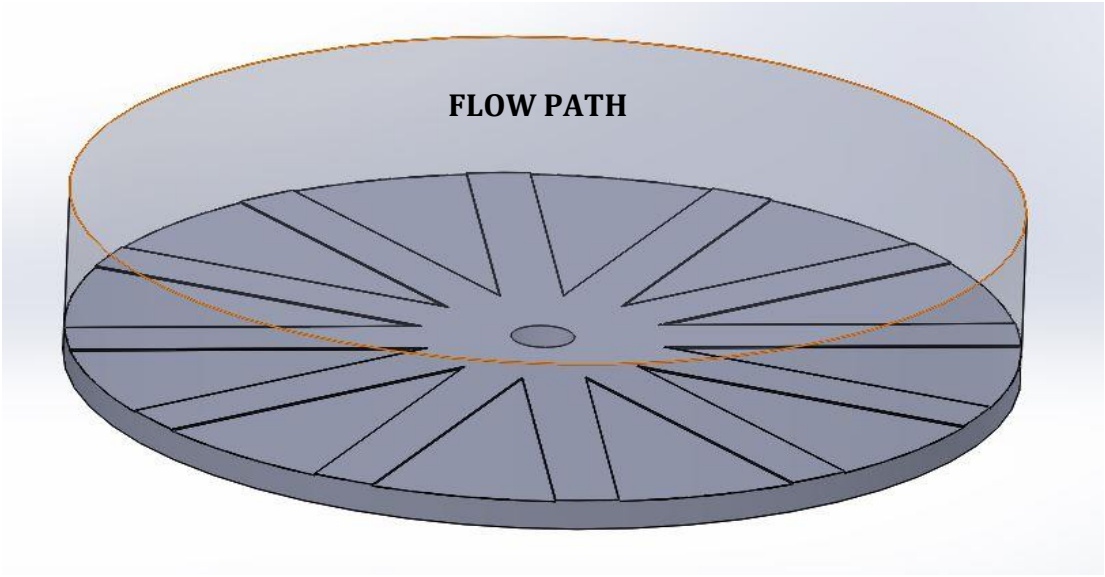

Fig 10. Rough disk and the flow path

In order to capture the complete effect of the roughness (it will also be mentioned as a *step*) it is necessary to create a geometry big enough so the step is contained inside (Figure 11):

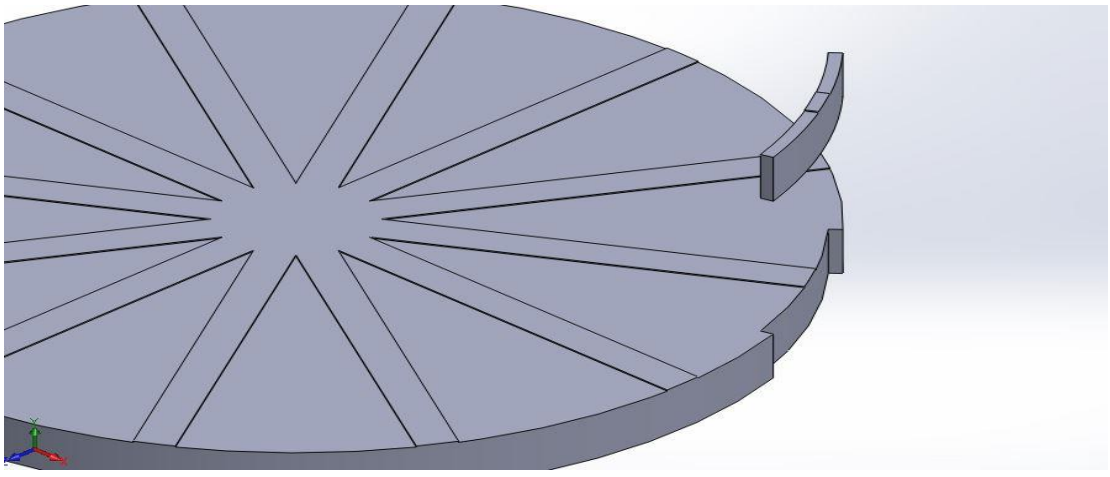

Fig 11. Differential domain of the rough disk

The step designed in the 2D flat plate is designed with the intention of achieving a high similarity with the disk, shown in the figure 12:

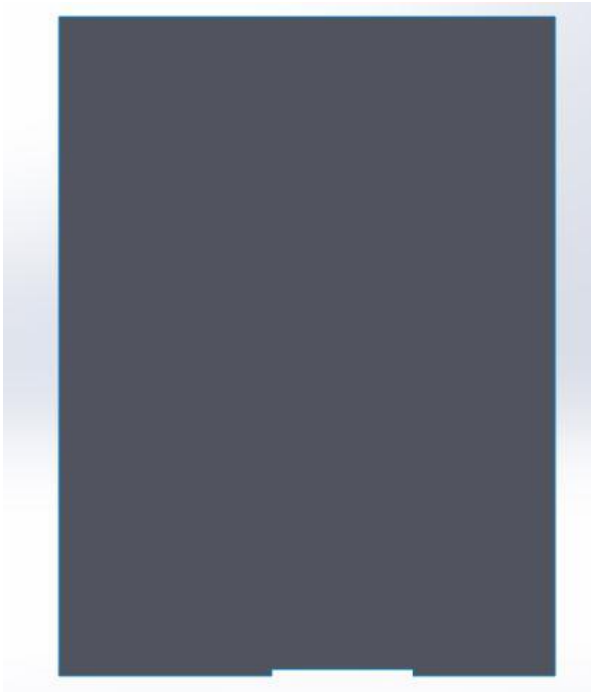

Fig 12. Domain of the rough flat plate

3.2 Spatial discretization: mesh

The first step in the application of computational fluid dynamics consists in the *spatial discretization* of the domain in order to be able to calculate a numerical approximation of the partial differential equations. There are many discretization methods of the problem and all of them require a previous geometrical discretization to perform the discretization of the equations that describe the fluid. There are, basically, two different types of mesh: structured and unstructured meshes.

Structured mesh: every point of the mesh is identified by the indexes *i, j, k* as Cartesian coordinates. The cells of the mesh are quadrilateral (2D) and hexahedral (3D).

Unstructured mesh: the cells and nodes from the mesh do not have any particular order, i.e. the cells or nodes close to a given one cannot be identified directly by their indexes. The elements of the mesh are, in this case, a mix between quadrilateral and triangular (2D) or tetrahedral and hexahedral (3D) elements.

In the case of study, an unstructured mesh is created by using the mesh generator software called ANSYS ICEM CFD. This software allows a great control over the mesh and using the proper parameters, the resulting mesh can achieve a really good quality, which is needed in order to obtain good results in the simulations. Coming up next, the creation of the mesh is explained step by step.
Once the geometry is created using SolidWorks, the file was saved as **.iges* file so the ICEM CFD software can import it.

3.2.1 Step 1: Defining edges and surfaces

First of all, different edges and surfaces on the geometries must be defined. Since the flat plate is two-dimensional, the control volume is surrounded by edges but the 3D rotating disk has surfaces instead of edges. Starting with the smooth rotating disk, the surfaces are defined as shown in the figure 13:

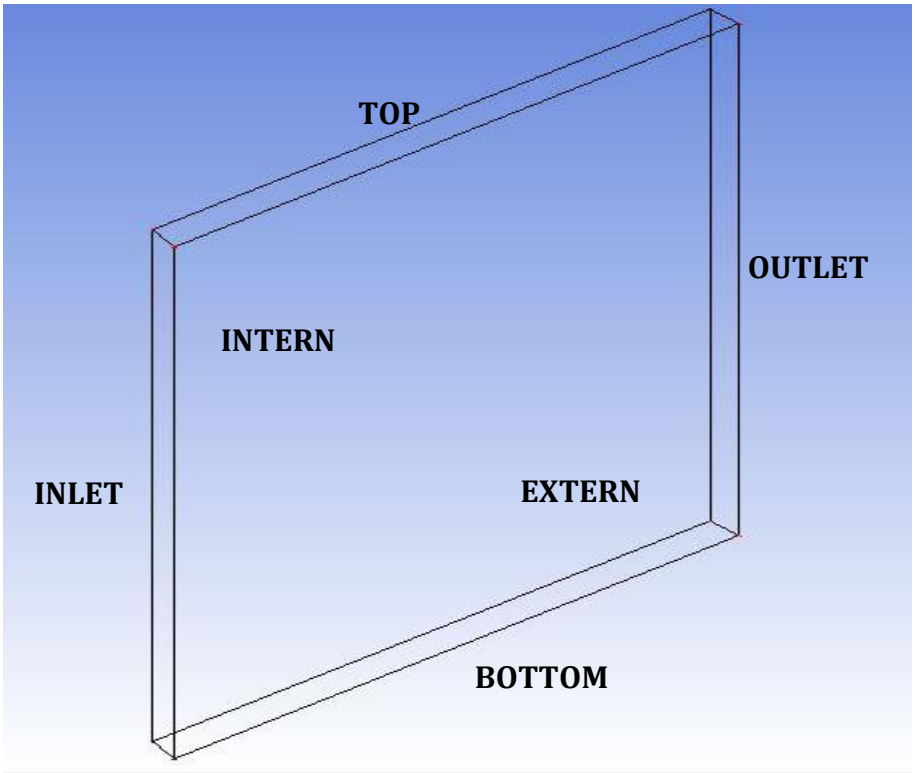

Fig 13. Surface naming. Smooth case

The *inlet* surface corresponds to the entrance of the flow inside the domain and the *outlet* surface defines through where the flow leaves the domain. The *top* surface corresponds to a fixed wall and the *bottom* surface is a moving wall. It has to be noted that there are three extra surfaces for the rotating disk with roughness. These three surfaces are called *roughness* and they are combined with the *bottom* in the simulating software, explained in the section 3.3.

For the flat plate case, the surfaces now turn out to be edges placed in the same position with the exact same names, but the surfaces *intern* and *extern* are no longer present.

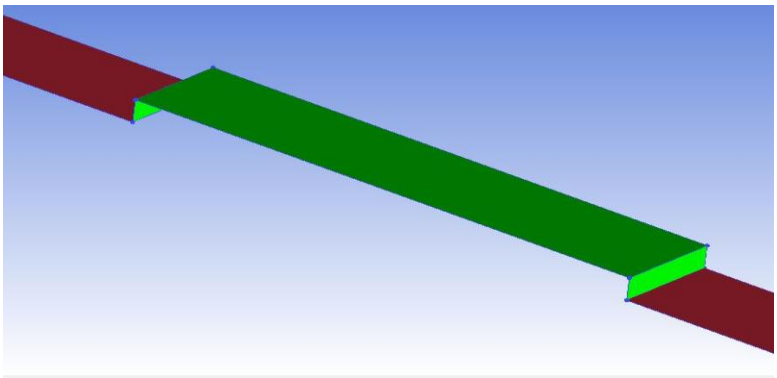

3.2.2 Step 2: Blocking and associations

The next obligatory step is the creation of a block containing the domain. In this chapter, only the rotating disk case is explained, since the flat plate case is very similar and simpler. The same method has been applied for both cases.

Although the creation of the block is enough for the smooth rotating disk (without the step), the creation of an *O-grid* is needed for the rough case. After the block is created, an *O-grid* is applied to the block. The reason of this is because a high resolution of the mesh is needed in the region close to the wall, and an *O-grid* gives a good control and precision of the mesh parameters on the desired region.

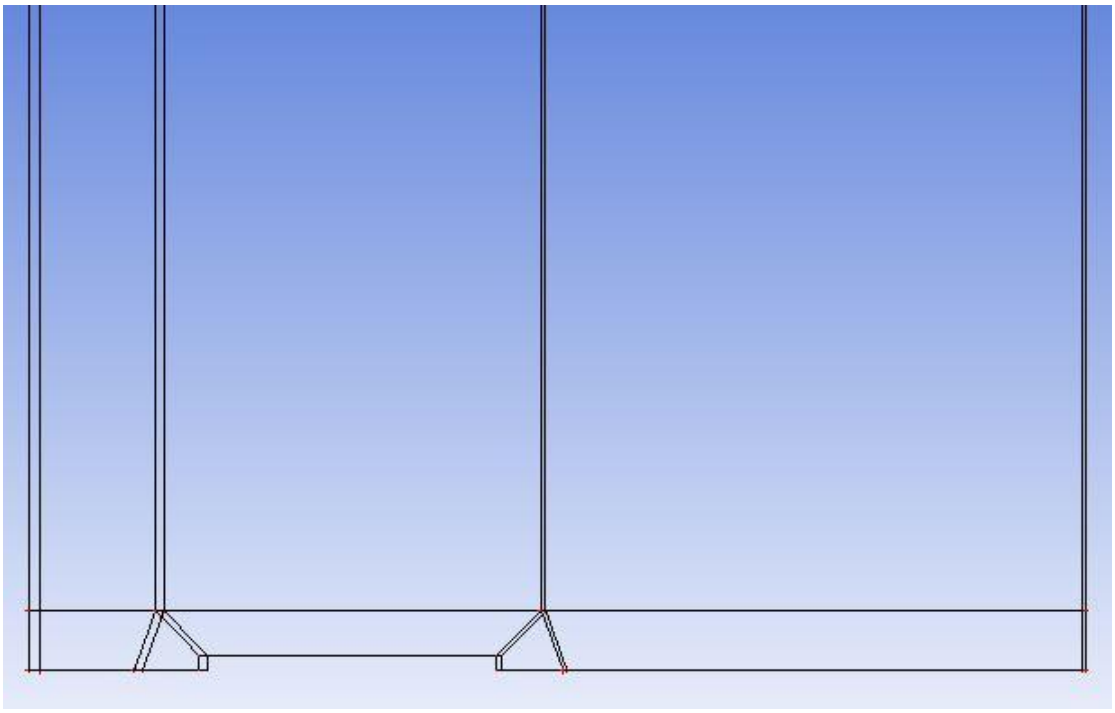

Fig 15. O-grid from the rough disk

Once the *O-grid* is created, the vertices of the block are associated to the vertices of the domain and after that, the same procedure is applied for the edges. The associations are the same for the smooth case, but there are less associations since there are less vertices and less edges. After the associations are done, it is time to define the parameters that define the mesh.

3.2.3 Step 3: Edge parameters and mesh

The CFD model used for the simulation demands a high refinement next to the wall. This refinement is translated to a y^+ value of the first cell equal or below 1 on both *bottom* and *roughness* surfaces. However, in order to achieve these y^+ values it is necessary to generate an initial mesh, simulate the case with this mesh and calculate the y^+ value of the first cell. If the value obtained is greater than 1, the initial mesh must be rebuild with a higher refinement. This is an iterative process that stops when the desired y^+ values are achieved.

The distribution of the nodes throughout the different edges has been done with the aim of a good precision in the close to the wall region but also minimizing the number of elements in the other regions where the refinement is not needed. For that reason, starting with the 2D flat plate, a *BiGeometric* law of distribution has been applied on the y-direction, providing good resolution on both bottom and top wall but minimizing the number of elements in the middle of the domain. By setting a value of 0.001 mm as the first node spacing and a 1.2 growth ratio for both initial and ending nodes, the edge is the one shown in the figure 16:

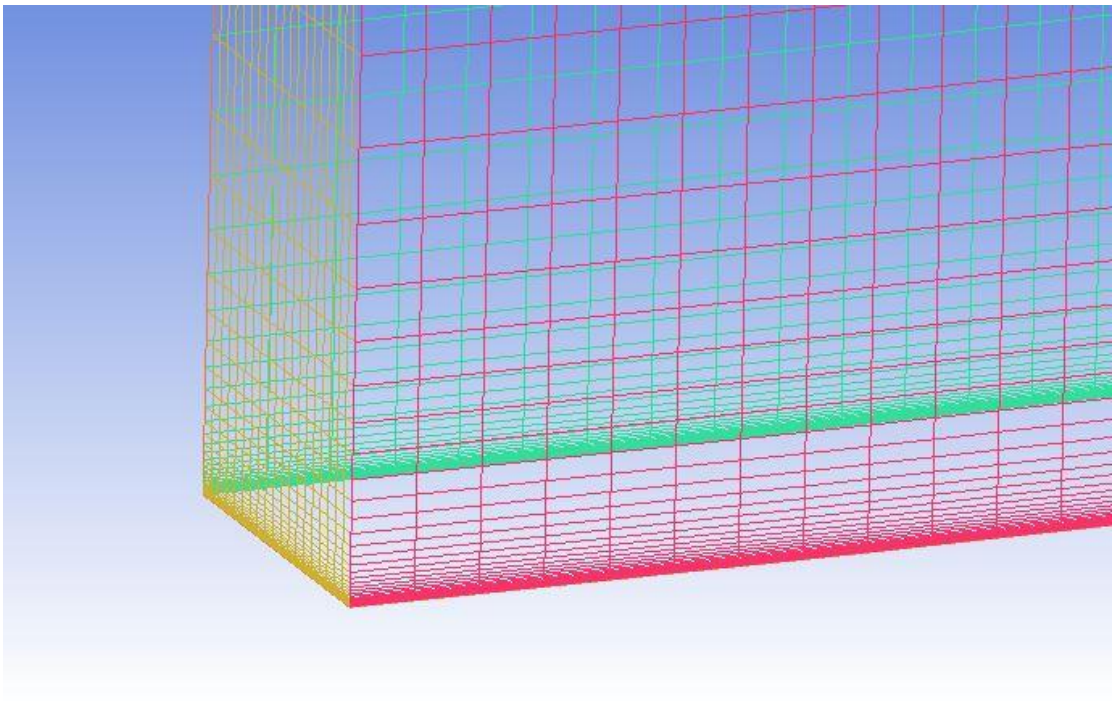

Fig 16. View of the bottom mesh from the disk

These meshes not only guarantee the previously mentioned y+ value of the first element below 1, but also a good quality mesh. The criteria used in order to consider a good or bad quality of the mesh have been: aspect ratio above 0.8, angles above 45 degrees and a 3×3 determinant of the elements above 0.8.

The rough cases have extra edges which come from the creation of the *O-grid* and the step, so edge parameters have been applied to them as well. The result of the *O-grid* leaded to this mesh:

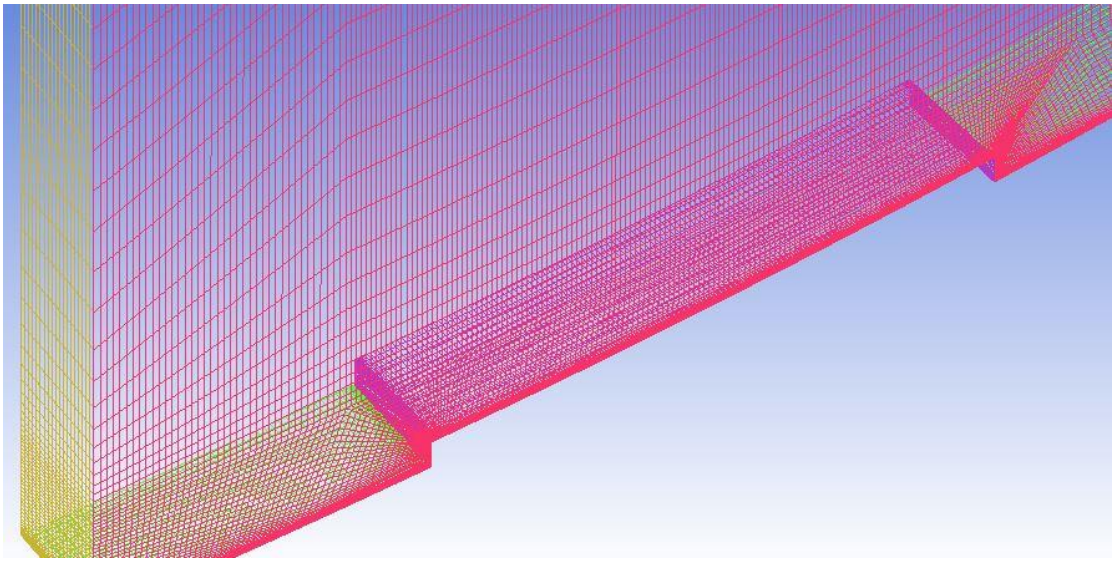

Fig 17. View of the mesh of the step. Rough disk

It is seen in the figure 17 that the refinement throughout the *bottom* and *roughness* is high maintaining a good quality mesh.

Before the mesh is ready to be exported to a CFD software program, the mesh has been transformed to an unstructured mesh which is red by the Star-CCM+.

3.3 Software settings: Star-CCM+

The simulations have been carried out with the CFD software program Star-CCM+. This software uses the mesh created in the previous section and simulates the domain with defined properties and boundary conditions which are explained next. Again, the section is divided in different steps easing the procedure.

3.3.1 Step 0: Importing mesh and combining surfaces

The first step is importing the mesh in format **.msh* from the ICEM CFD to the Star-CCM+. After that, the two different surfaces defined in the ICEM CFD as *bottom* and *roughness* (only for the rough cases) are combined into one. The reason is that both surfaces represent the same object (surface of the plate or disk) and therefore, both have the same boundary conditions. The new surface is called *WALL*.

3.3.2 Step 1: Model properties

The model properties are listed below, which are believed to be accurate describing the fluid of study:

- Turbulent model: $k-\omega$ model with SST
- Steady flow
- Low Y+ wall treatment
- Constant density

- Liquid
- Segregated flow solver

3.3.3 Step 2: Boundary conditions

A proper definition of the boundary conditions leads to reasonable and correct results on the simulation.

For both cases, the conditions on the INLET and OUTLET are not significant since an interface between those regions was created. Since the domain is a small representation of the full geometry (full disk or full flat plate), a periodic transformation must be done. After this interface is created, the simulation runs as if the flow leaving the domain through the OUTLET region enters to the domain again through the INLET region. This is equivalent as if infinite identical geometries were placed one after another, leading to the geometry that is wanted to be studied. The properties of the surface are:

- Periodic transformation with a zero pressure gradient
- Fully developed flow
- Transformation:
  - Linear transformation with an offset of [35 0 0] for the flat plate.
  - Rotating transformation with an axis placed in the (0,0,0) and the direction [0,1,0].

Once the interface is created, the periodic transformation is applied to both regions and the conditions specified before (velocity inlet and pressure outlet) are no longer active.

- The final boundary conditions of each region are defined as follows:
  - **FLAT PLATE**
    - TOP: fixed wall with no-slip condition.
    - WALL: moving wall with a lineal velocity in the *x* direction of 7.85 m/s. No-slip condition.
    - INLET: periodic.
    - OUTLET: periodic.

  - **ROTATING DISK**
    - TOP: fixed wall with no-slip condition.
    - WALL: moving wall with a rotating speed of 500 rpm along an axis placed in the (0,0,0) and direction [0,1,0]. No-slip condition.
    - INLET: periodic.
    - OUTLET: periodic.
    - INTERN: fixed wall with slip condition.
    - EXTERN: fixed wall with slip condition.

The reason why the slip conditions are defined in both EXTERN and INTERN regions is that there is also flow outside the domain with the exact same

properties, so the contact between the exterior flow and these two regions do not generate any shear stress and therefore, there is a slip condition.

3.3.4 Step 3: Initial conditions and monitors

The initial pressure and velocity values only have an effect on the convergence of the simulation, but not on the results. However, a value around 7.8 m/s and 0 Pa is recommended.

Additionally, a few monitors were created in order to obtain data which is explained in the Chapter IV. One of the characteristics of the boundary layers that are studied are the Reynolds stresses (in this case, only the one on the first principal direction) and it is necessary to create Variance monitor for the *streamwise* component of the velocity.

Another monitor that controls the evolution of the wall shear stress is also created, as it is used as a convergence criteria.

3.3.5 Step 4: Solvers and convergence criteria

A $k-\omega$ turbulence model was used in both cases. A segregated flow solver is used in the simulations not only because it gives good results but also because it has a higher resolution speed than the coupled flow solver, which is mostly used on simulations with compressible flows. The convergence of the simulations are based on 2 criteria explained on the next chapter (Chapter IV), so the number of iterations may differ from one simulation to another. The range of iterations for all cases go from 10.000 up to 1 million.

3.3.6 Step 5: Post-processing

The study is focused on the boundary layer so results along all the boundary layer are needed. In order to get those results, planes parallel to the WALL region were created at different distances from the WALL. The number of planes and therefore, values inside the boundary layer, is around 100.

The values were obtained by the creation of different reports that calculated the desired properties on the planes. These were the reports created:

- Streamwise velocity component [i] for the flat plate case.
- Velocity component [tangential] for the rotating disk case.
- Vorticity around axis normal to 2D plane [k] for the flat plate.
- Vorticity [radial] for the rotating disk.
- Y position for both cases
- Variance of streamwise velocity component [i] for the flat plate
- Variance of velocity component [tangential] for the rotating disk.

Usually, the velocity profiles shown in the reports and books are based on the assumption that the flow is moving throughout a fixed wall. However, given the boundary conditions of the model, the velocity profile obtained would be different (reversed). For that reason, a transformation of the variables has been

done, so the profile obtained can be easily compared to the ones seen in the books.
The transformation is simple and it is basically a change of reference. The maximum velocity is initially at the bottom wall, while the minimum velocity is at the top wall.
By using this formula:

$$u_{ref} = u_{wall} - u_{ini} \tag{35}$$

Where u_{ref} is the velocity on the new reference, u_{wall} is the maximum velocity (at the bottom wall) and u_{ini} is the velocity obtained initially, before doing the transformation. Now, the plot obtained has a more familiar shape.

4 Chapter IV: CFD results

In this section, the results obtained from the CFD will be presented. Since one of the main objectives of this project is to find a possible similarity among some of the parameters inside the boundary layer, it is interesting to compare each case of roughness between the flat plate and the rotating disk.

The validation of the results is of utmost importance. It is necessary to establish different criteria which will guarantee that the solution has reached convergence, i.e. the solution does not change. Since the cases have different conditions, different meshes and different geometries, the number of iterations may vary in each case, making the number of iterations useless as a convergence indicator. For instance, the simulations with the lowest number of iterations had around 30.000 iterations, whereas the simulation with most iterations had over 1 million.

It is explained inside the methodology section that a wall shear stress monitor was created in order to see the evolution of the wall shear stress. The wall shear stress criterion will be considered satisfied when it reaches an approximately constant value.

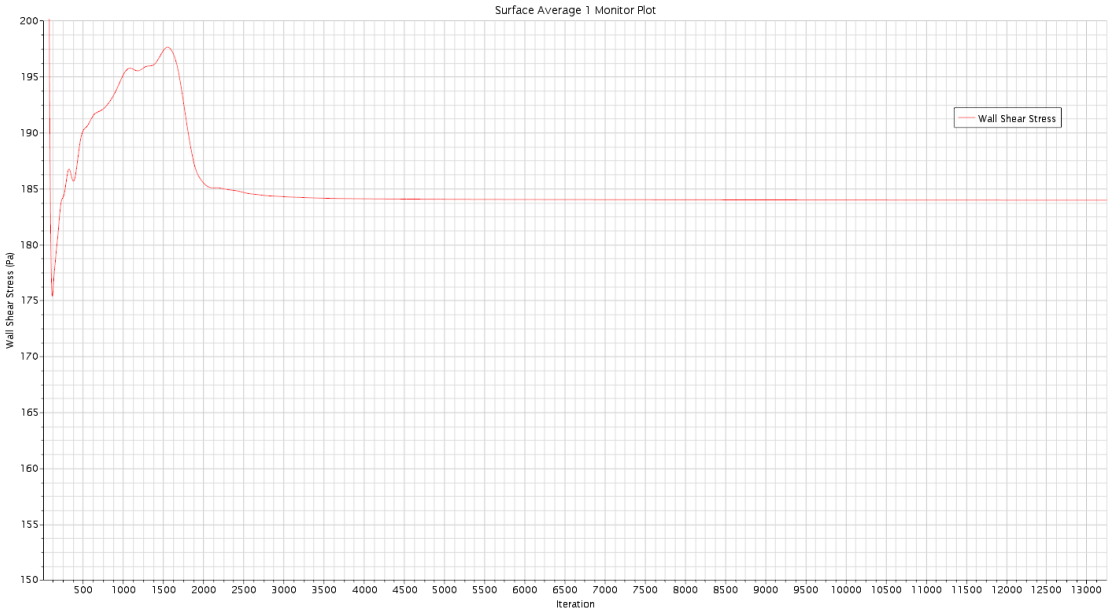

Fig 18. Monitor plot of the wall shear stress

The wall shear stress will be considered constant if this condition is satisfied:

$$\frac{\tau_{w,n} - \tau_{w,n-1}}{\tau_{w,n-1}} < 0.0001 \qquad (36)$$

Basically, the previous formula is limiting the difference of the last value and the previous value, which will be considered as 0.01%. In all cases, this condition is imposed in order to consider the solution converged.

In addition, the residuals are taken into account as another convergence criterion, which must be satisfied. Since the residuals will not remain constant and their values change significantly on every iteration, it will be set as a condition when the residual values are below 10^{-3}, as shown in the figure 19:

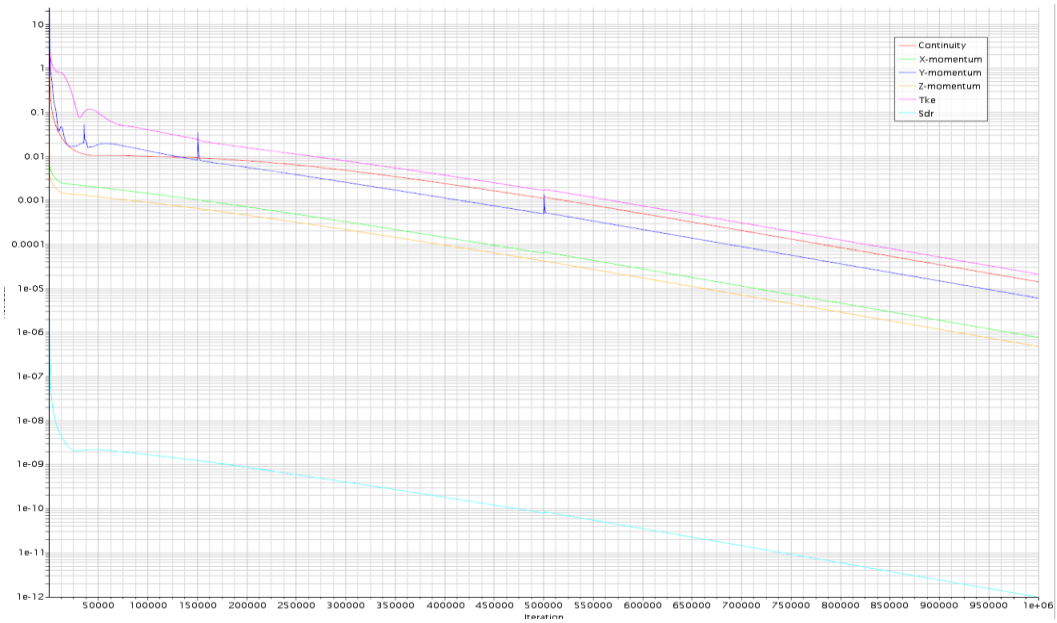

Fig 19. Plot of the residuals

Even if these two criterions are satisfied, it is recommended to check the contour velocity plots, which give an idea of how the fluid is flowing through the domain. Since the case of study is not completely new, one can expect some shapes inside this plot. Thus, checking these plots can also be useful in order to see how reliable the simulation and the results can be.

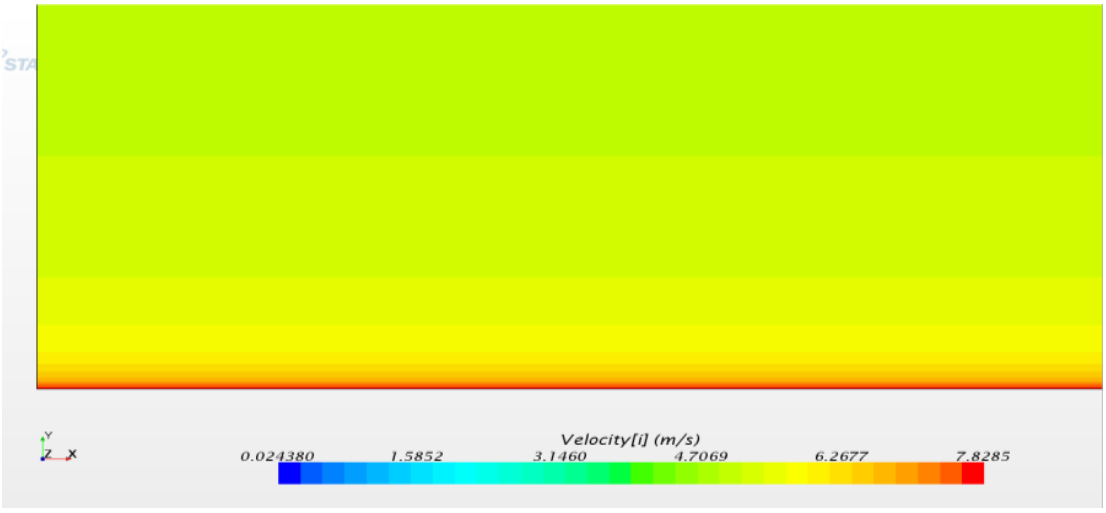

Fig 20. Velocity contour plot. Smooth flat plate

In the figure 20, it can be seen that the bottom wall is moving with the velocity set up on the software, dragging the fluid and generating the boundary layer. The velocity decreases as we move away from the wall due to the viscosity effects explained in the theory chapter. It is not possible to have a clear idea of the velocity profile with this plot, but according to the theory and the boundary conditions, it should be a Couette flow. However, further inside this section, different plots will be shown which will give a clear idea of those profiles.

The following case introduces a small step in the geometry, which affects completely the boundary layer and the flow path, shown in this figure:

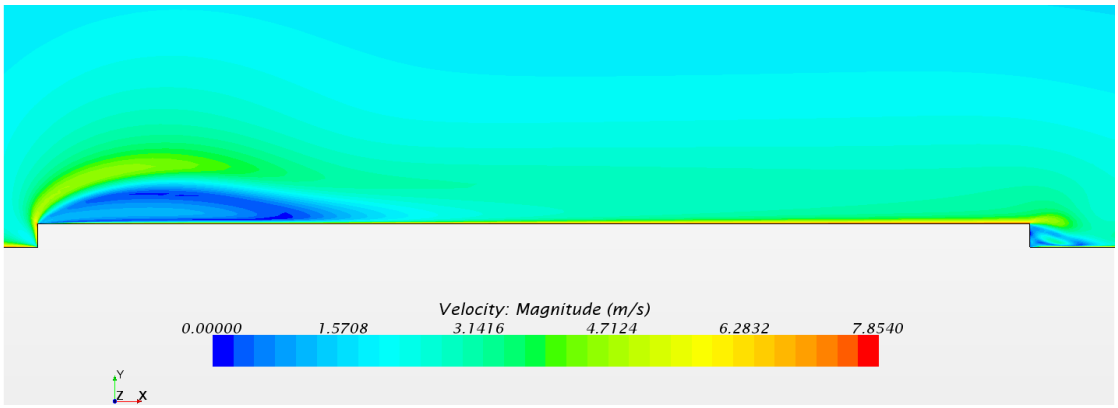

Fig 21. Velocity contour plot. Flat plate roughness 1

In figure 21, the fluid travels freely through the domain until it encounters the step, which makes the flow change its direction to surround the step. This generates a recirculation both at the beginning of the step and the ending of the step (darkest blue zones). It can also be seen that the closest region to the wall is red colored, which means that the wall is moving with the desired velocity.

According to the Antonia and Luxton [17], as the height of the step is increased, the recirculation of flow on both regions should increase, and the size of the recirculation increase too. This idea is reflected in figure 22:

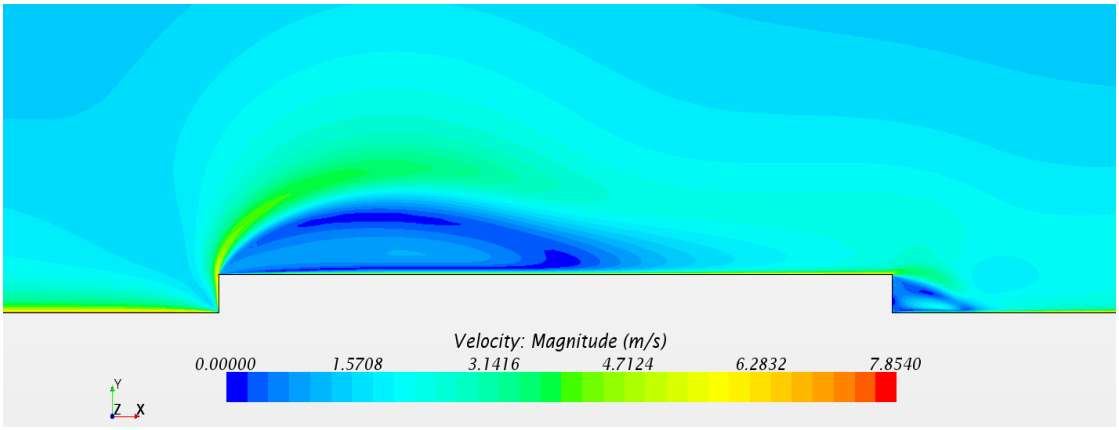

After checking the residuals and the wall shear stress monitor plots, the solution can be assessed and we can determine whether the results are reliable or not.

It must be noted that the velocity vectors in the *flat plate* are two-dimensional, whereas the velocity vectors of the *rotating disk* case are three-dimensional. However, only one component of each vectors is post-processed and compared, since it is expected to find the strongest similarities. The components compared are the *streamwise* component velocity (direction of the moving wall) of the flat plate and the *tangential* component of velocity of the rotating disk. Even though the other components are not zero, the contribution of velocity to the vector velocity is small enough to be neglected.

Fig 22. Velocity contour plot. Flat plate roughness 2

4.1 Comparison: velocity contour plot

A first approach in the comparison between the flat plate cases and the rotating disk cases is the visual comparison of velocity contour plots. If the initial hypothesis is correct, both plots should have, at least, some similarities. The plots will be matched in pairs depending on the roughness.

4.1.1 Smooth surface

We will begin with the simplest case, the one with smooth surface.

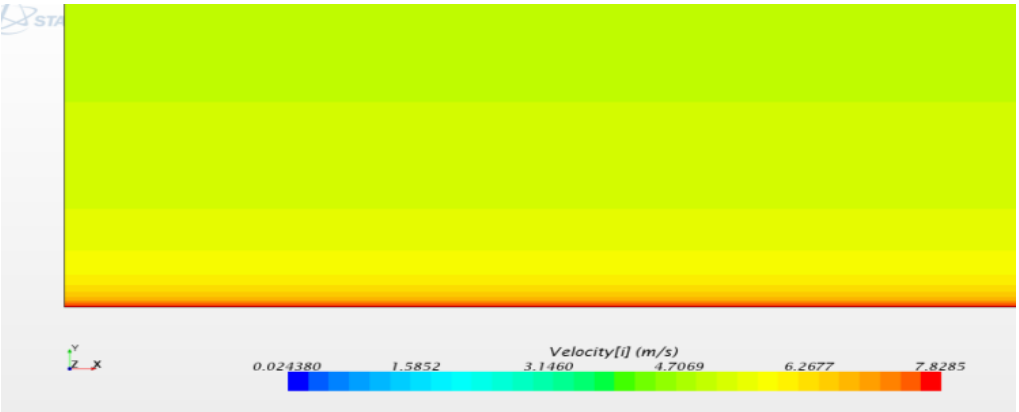

Fig 23. Velocity contour plot. Smooth flat plate

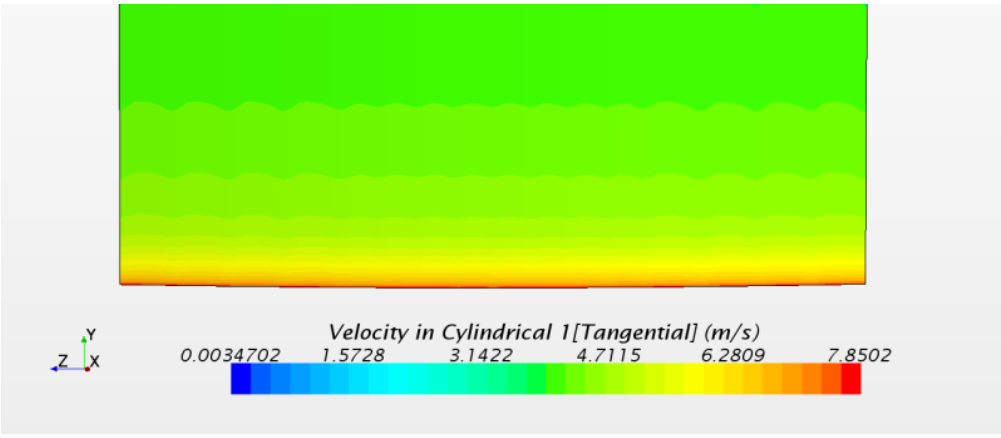

Fig 24. Velocity contour plot. Smooth rotating disk

In figures 23 and 24, the velocity of each element is represented by a different color (see the scale bar of velocities). As the distance from the wall increases, the velocity of the element decreases gradually. It can be observed that, even though the colors that represent the velocities are not distributed in the exact same way, there is a significant similarity on the velocity gradient in the *y* direction, i.e. there is a reduction of the velocity the more it moves away from the wall.

4.1.2 Small roughness

It was seen at the beginning of this section, that as soon as the roughness appears in the geometry, the flow starts to recirculate in two zones of the domain. On both cases, the shape and size of the recirculation is very similar.

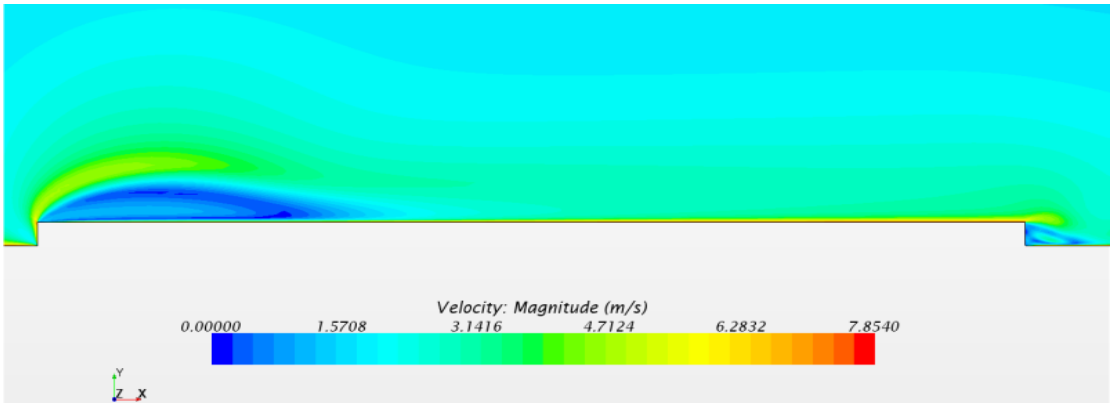

Fig 25. Velocity contour plot. Flat plat with roughness 1

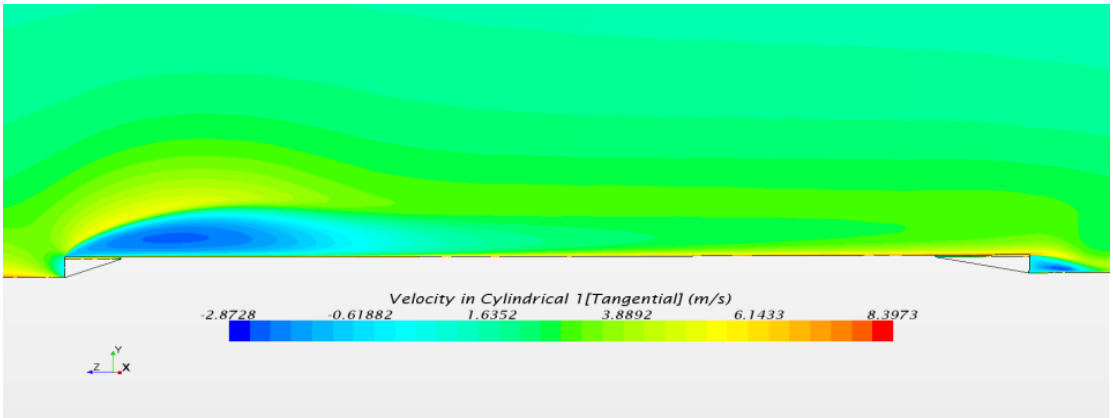

Fig 26. Velocity contour plot. Disk with roughness 1

The colors in figures 25 and 26 are significantly different, and there is an explanation. If one looks at the color bar with the range of velocities, the maximum velocity on the flat plate is 7.85 m/s (the one used in the set up), while on the rotating disk, the maximum velocity is 8.4 m/s. The fact that the maximum velocity on the disk is higher is because there is a stagnation point near the beginning of the step, where the velocity is higher than the velocity of the free stream. For that reason, all the velocities have the colors rescaled. However, as it will be seen in the following sections, the profiles will still be very similar.

4.1.3 Big roughness

Once again, the results obtained by increasing the height of the step are as expected, as it can be seen in figures 27 and 28.

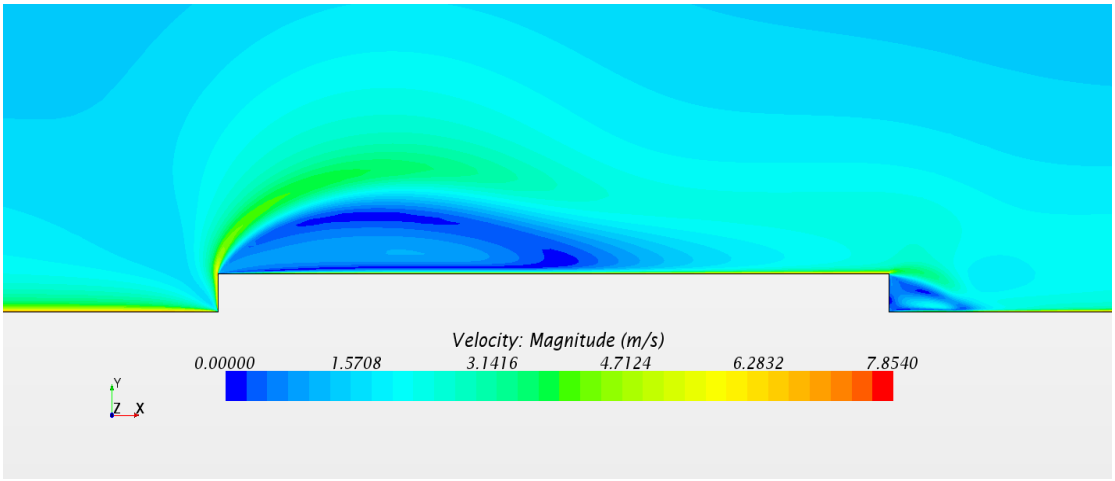

Fig 27. Velocity contour plot. Flat plate with roughness 2

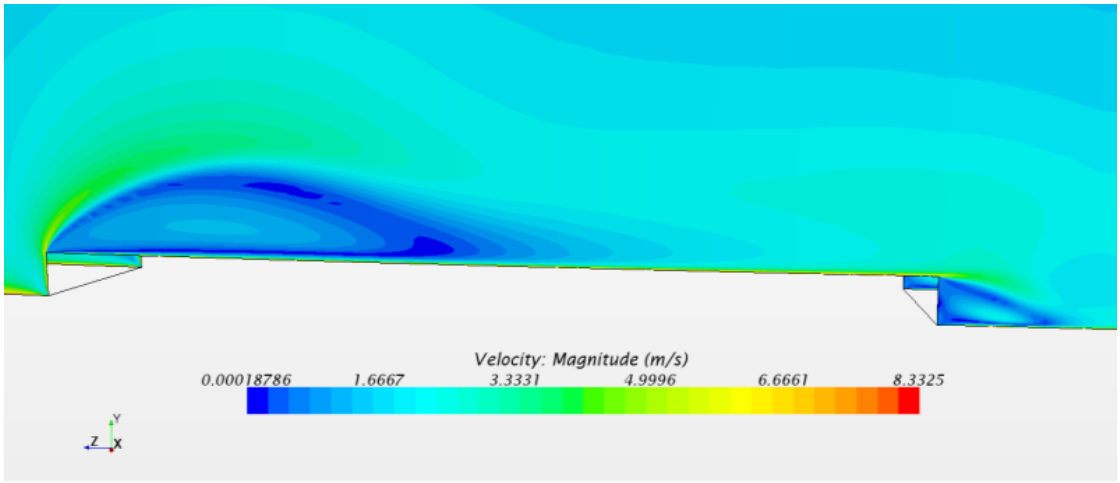

Fig 28. Velocity contour plot. Disk with roughness 2

The effect of the new height on the size of the recirculation is the same for both cases. It should be noticed that the effect mentioned by the stagnation point on the previous case is present in this one as well.

4.2 Logarithmic law layer

A comparison between the logarithmic laws (*log-law*) of each case will be shown in the same plot. On one hand, it will help to understand how the roughness affects the *log-law* and on the other hand, the similarity of the curves between the cases. The values plotted correspond to the values of the different planes created on the Star-CCM+ (explained in the section 3.3.6) and they are shown in the figure 29:

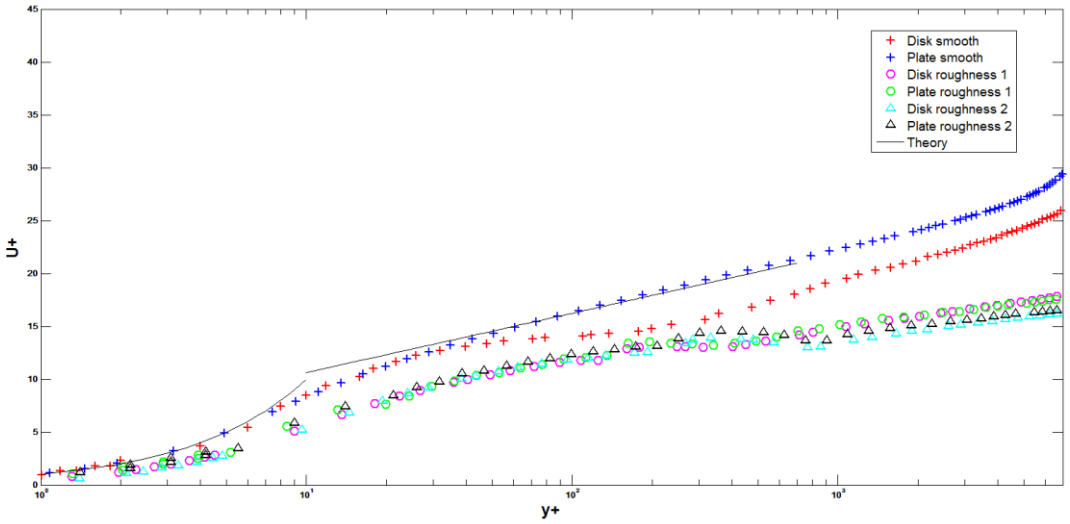

Fig 29. Law of the wall plot. Log-law

From now on, the colors and symbols will be the same for each case, trying to facilitate the analysis. For each paired case (smooth, roughness 1, roughness 2) the same symbols have been used in order to make visual analysis easier. The *Plate smooth (blue)* curve has a very similar profile as the theoretical curve, what gives reliability to the results obtained. The only difference observed between the blue curve and the *Disk smooth (red)* curve is a small offset, but the curves are parallel inside the *log-law* region.

As expected for the small roughness case (circles, pink and green), the curve is displaced downwards. The offset between the plate (green circle) and disk (pink circle) curves now decreases, obtaining almost equal curves for both roughness. According to the theory, an increase of the height of the step causes a higher displacement downwards of the curve. The big roughness (triangles) has twice the height of the small roughness (circles), and it can be seen in the plot that the curves for the second roughness (triangles, magenta and black) are under the first roughness. However, with only two different roughness and being those height values not very differentiated, it is not possible to estimate the behavior of the *log-law* with a considerable higher step.

4.3 Velocity profiles

For the smooth case, a Couette velocity profiles is obtained as expected, shown in figure 30:

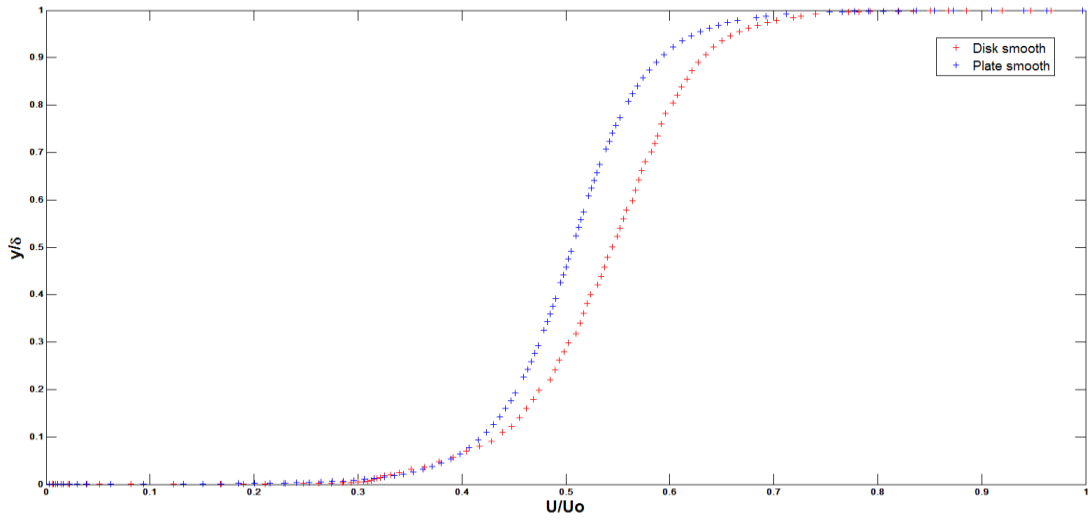

Fig 30. Velocity profiles. Smooth cases

A perfect anti-symmetric profile is obtained with the *flat plate* case as the flow is a Couette flow. Although the *rotating disk* profile is not completely anti-symmetric, the similarity between both curves is considerably high. One possible explanation for this offset is related to the simplification previously done, where both axial and radial components of the *rotating disk* vector velocity are not considered.

Once the roughness is introduced, the profiles are not symmetric anymore, which could indicate that the flow does not behave like a Couette flow anymore.

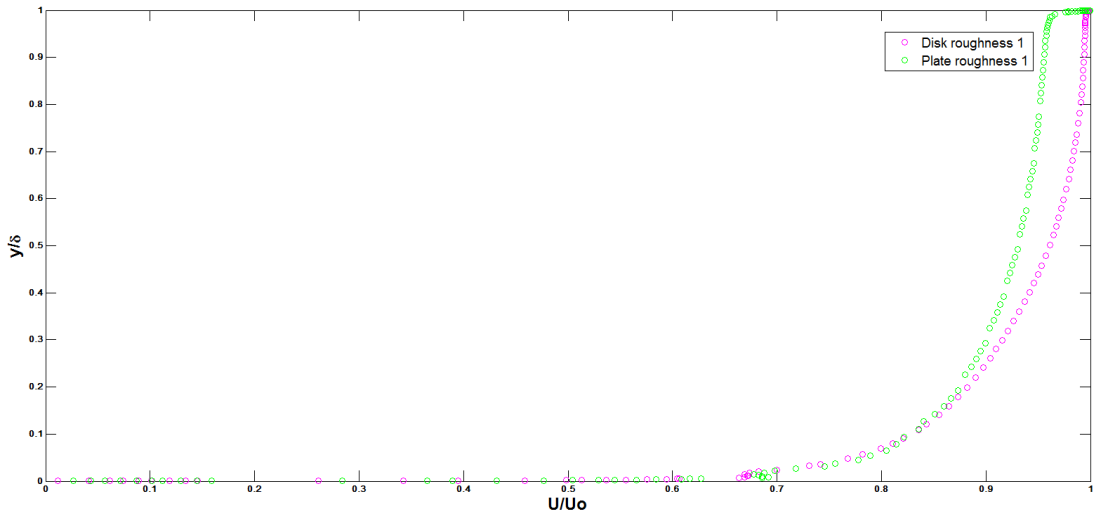

Fig 31. Velocity profiles. Roughness 1 cases

As it can be seen in the figure 31, for both cases the curve are much flatter close to the wall. The offset between the curves is still present, but its value is considerably small. Nevertheless, when the roughness grows obtaining the second roughness case, this offset decreases, obtaining almost equal curves, as shown in the next figure:

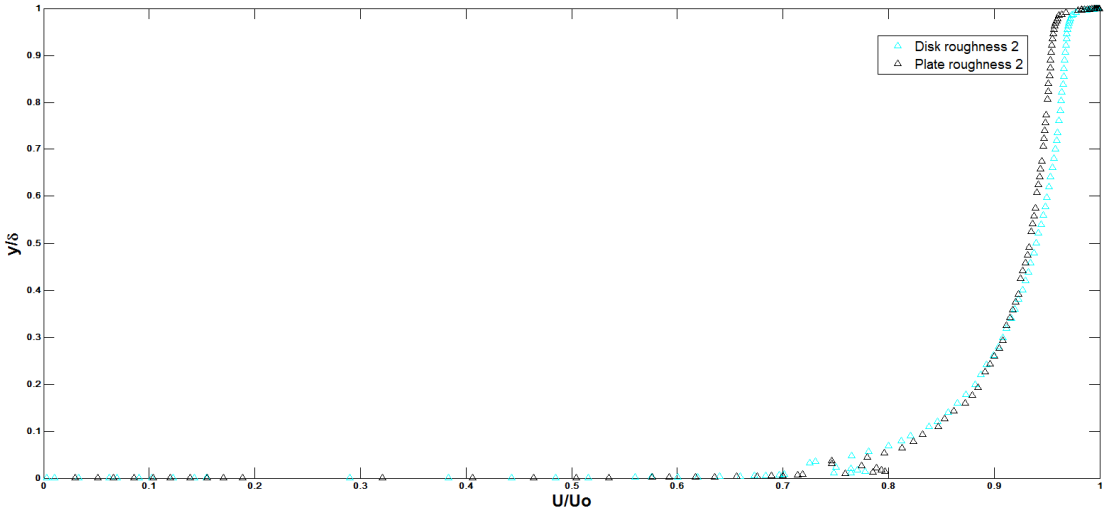

Fig 32. Velocity profiles. Roughness 2 cases

As seen in the figure 32, on both rough cases there is a perturbation at low y/δ values due to the acceleration the flow suffers when it encounters the step. Since the height of the second step is bigger, the acceleration is bigger which places the perturbation more to the right. For the exact same reason, the y/δ value of the perturbation is higher as well for the second roughness.

4.4 Vorticity profiles

The vorticity is strictly related to the turbulent behavior of a flow. For that reason, plotting the vorticity is considered of utmost importance.

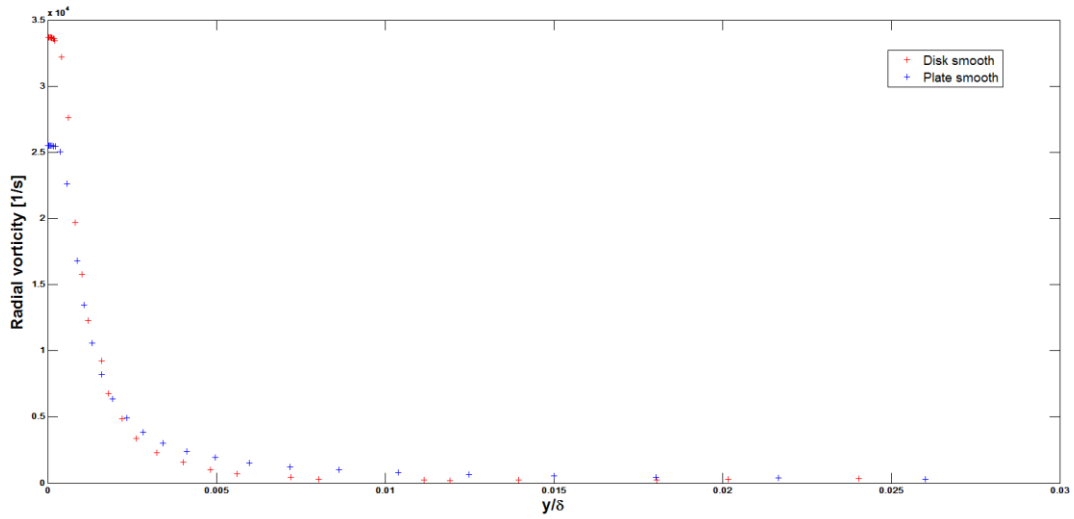

Fig 33. Vorticity profiles. Smooth cases

As seen in the figure 33 the biggest differences are found in the smooth case. However, even though the vorticity values very close to the wall have an offset of $0.75 \cdot 10^4$, the shape of the curve is very similar as soon as we move away from the immediate close wall.

Given the changes observed in the velocity profiles plots, it is not surprising that the curves with both small and big roughness are more similar than the smooth curves:

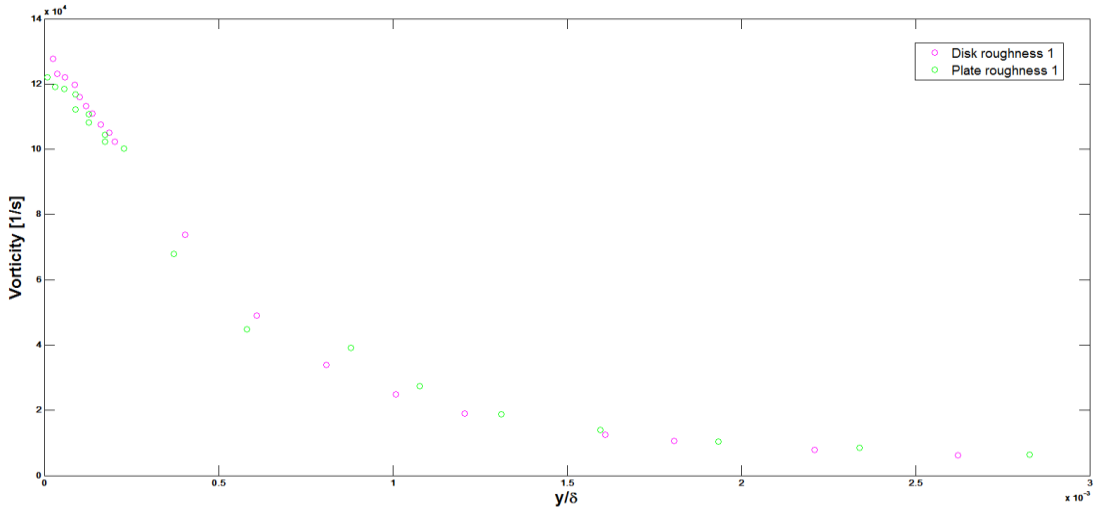

Fig 34. Vorticity profiles. Roughness 1 cases

Figures 34 and 35 corroborate the ideas seen in the vector contour plots (figures 27, 28, 29 and 30), where it was deduced that the recirculation was higher not only in size but also shape with the roughness 2 than in the roughness 1.

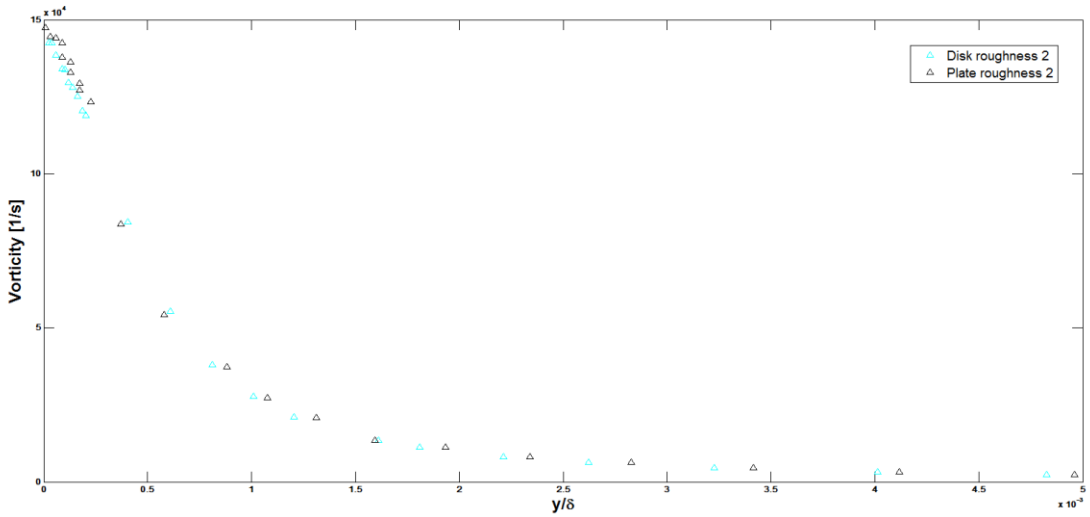

Fig 35. Vorticity profiles. Roughness 2 cases

4.5 Reynolds stress $\overline{u'u'}$

The study of friction and drag forces over the flat plate is essential, as it was mentioned in the motivation of this project. For this reason, a comparison between the Reynolds stresses is necessary. In order to consider that the stresses present on a flat plate and a rotating disk are the same, a similarity between the stresses on both cases should be found. Since the model used is a RANS model, all directions have the same Reynolds stress (considered isotropic) so it will be only shown the Reynolds stress on the direction of the flow.

The Reynolds stress values are obtained by plotting the values of the Variance monitor created for the streamwise component of the velocity:

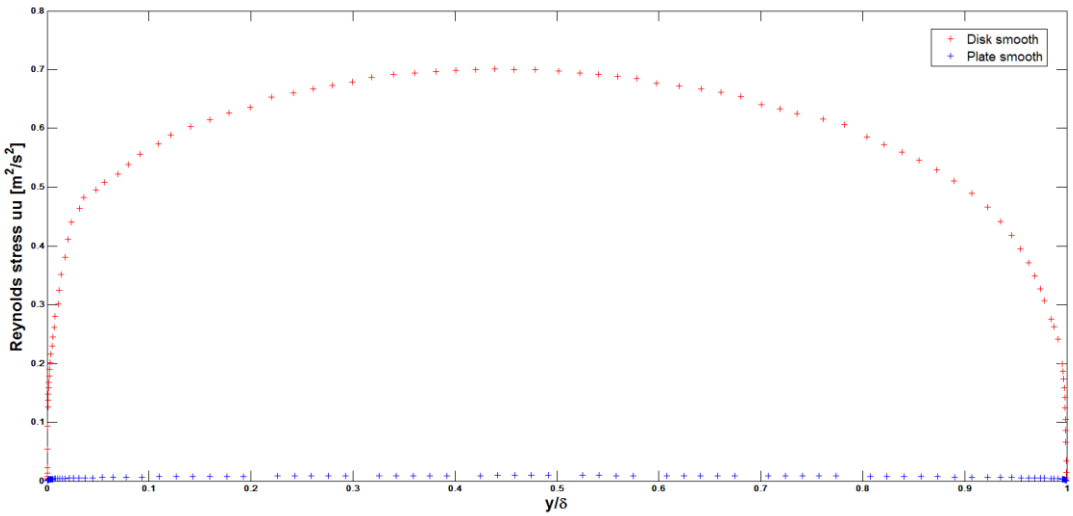

Fig 36. Reynolds stress $\overline{u'u'}$. Smooth cases

The Reynolds stress in both cases (plate and disk) is symmetric due to the symmetry of the domain. However, significant differences were found between the values.

For the roughness cases, the following curves were obtained:

Fig 37. Reynolds stress $\overline{u'u'}$. Roughness 1 cases

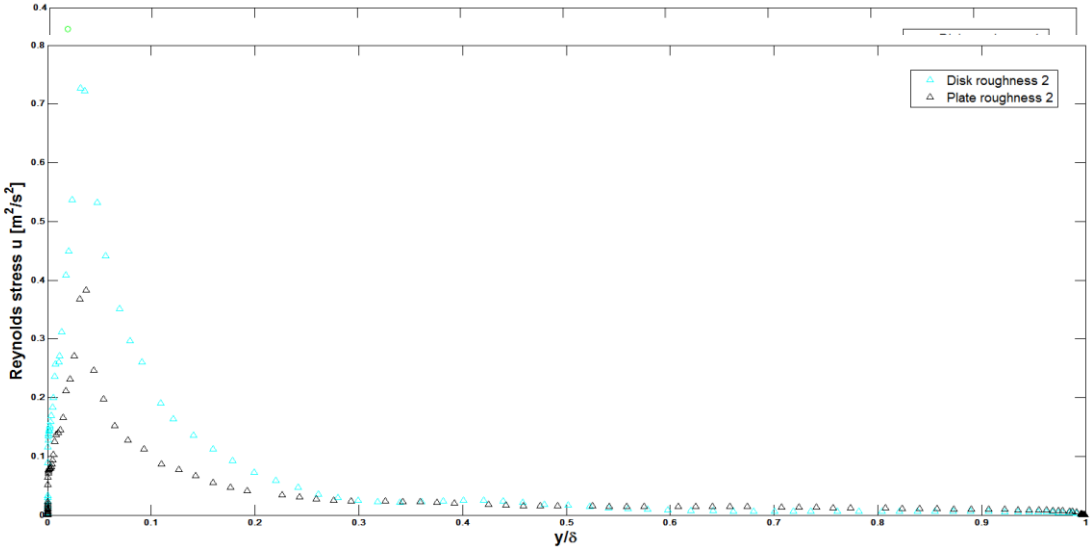

Fig 38. Reynolds stress $\overline{u'u'}$. Roughness 2 cases.

In figures 37 and 38, not only the curves on each figure have again very similar shape, but also the peak of Reynolds stress appears on the same y/δ values, and these are close to the y/δ values of the step. It can be deduced then that the transmission of shear stress between the flow layers follows the same pattern in the *flat plate* case and the *rotating disk* case.

5 Chapter V: Experimental procedure

It is important to validate the results from the CFD simulations. Therefore, taking advantage of the fact that a rotating disk rig was available due to experiments carried out for another project, we wanted to compare the numerical results with experiments. Throughout this chapter, the methodology and procedure for the experiments will be explained. The conditions for both CFD simulations and experiments are similar, expecting similar results. Experiments were done only for the rotating disk case, so the experimental methodology is focused on the disk and not on the plate.

5.1 Designing the tank and shaft

A special tank was designed for this experiment. Minimizing the volume of flow contained inside was intended, reducing the volume up to 20 litters. A more accurate visualization of the tank will be added in the appendix section, with the drawings needed in order to build the tank.

The distance between the walls and the disk surface is a parameter that must be taken into account. If the chosen value is too small, the development of the boundary layer can be affected by the walls. Previous studies [18] have shown that a distance higher than 20 mm is enough so there is no interaction between the walls of the tank and the boundary layer's generation. Also two openings were designed easing the access inside the tank, so the disk can be switched with the other 2 disks (3 disks under study: smooth, roughness 1 and roughness 2). Both openings are sealed, avoiding the leaking of the fluid.

A special shaft was designed as well, in order to facilitate the measurements and the connection between the devices of the hot-film anemometry, which collet the data, and the surface of the disk. Drafts and images from the design can be found on the appendix.

5.2 The rig

The assembly is composed by few different parts. The rig designed using SolidWorks can be seen in the figure 39 and consists of an electrical motor (with a controlled speed) connected to the shaft. Along the shaft, the hot-film anemometry devices are found, with a wireless device which sends the registered data to a computer. At the end of the shaft, the disk is rotating inside the tank, dragging the fluid inside it. The disk is placed exactly in the middle of the tank, so the minimum distances between the edge of the disk and each wall are the same. As mentioned before, the rig was available and just needed a new tank and shaft for carrying out these experiments.

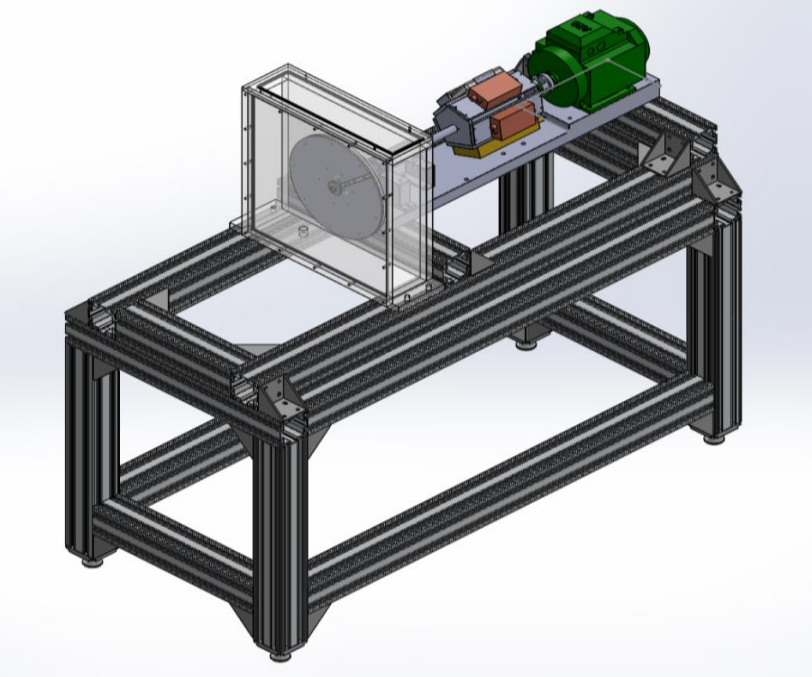

Fig 39. Experimental mounting

5.3 Measurements: Hot-film anemometry

The measurements in the experiment were performed using a hot-film anemometry. Three different sensors were placed on the surface of the disk at three different distances from the center in the radial direction: 5, 10 and 15 cm. Since the partial domain of the disk simulated corresponds to the edge of the disk, the simulated results have been compared to the experimental results from the third sensor, the one placed at the edge. One of the limitations this measurement procedure has it the fact that measures can only be done at the wall (surface of the disk) and not throughout all the boundary layer.

5.4 CFD results compared with experiments

The Hot Film anemometer is commonly used in fluid dynamics research, but one downside of using this experimental technique is its high sensitivity to the conditions (temperature and contaminants) of the fluid that will be used for the experiments [19]. Within the project, these experimental conditions might not be carefully monitored and therefore, there are reasons to believe that the data obtained from these experiments lack of enough reliability to obtain relevant information. However, the validation of the CFD results was still desirable. Thus, a well known experimental relation to estimate the skin friction over a flat plate was used, which is the ITTC-57 equation [20]:

$$C_{f,exp} = \frac{0.075}{(log_{10} Re_{exp} - 2)^2} \tag{37}$$

Where Re_{exp} is the experimental linear Reynolds based on the tangential velocity of the disk:

$$Re_{exp} = r\sqrt{\frac{\omega}{\nu}} \tag{38}$$

Being r the radius of the disk, ω the rotational speed and ν the kinematic viscosity. As the value of this Reynolds number is always known because the rotational speed and radius are known, the skin friction is possible to be estimated and in figure 40, the resulting plot of the skin friction obtained from both the simulations and the ITTC-57 equation is shown.

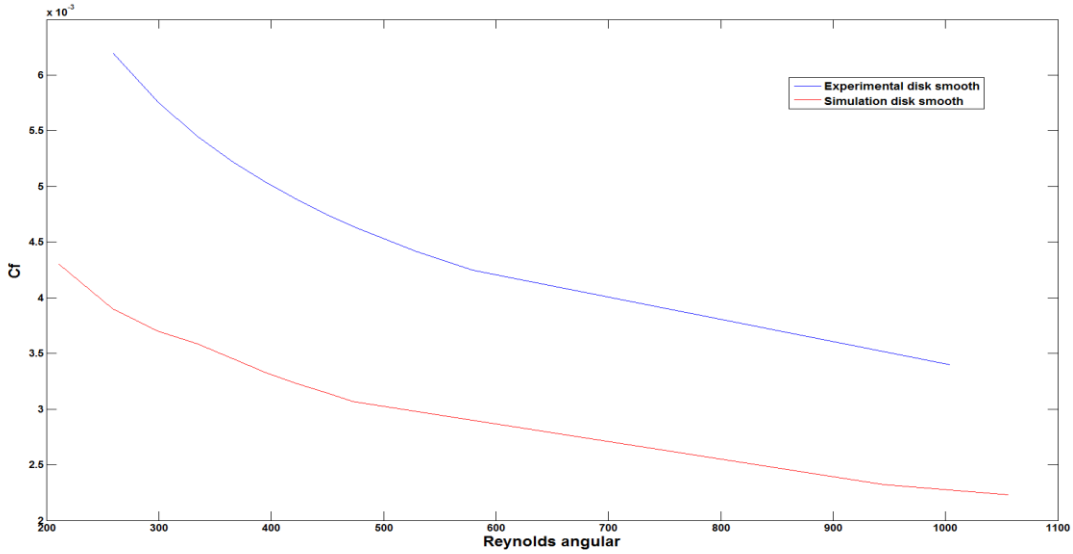

Fig 40. Skin friction coefficients from the ITTC-57 equation and CFD

As it is observed, the skin friction values are lower when predicted by the CFD simulations, compared to the skin friction calculated from the ITTC-57 formula. Although the values for this parameter are not similar in both methods, it is interesting to note that the behavior of the curve is almost the same for both cases and as we expect, with higher angular Reynolds number, the C_f decreases asymptotically. Since the $C_{f,exp}$ is based only on the tangential velocity, the values are the same for the rough disks (same radius and same rotational speed). The ITTC-57 equation does not include the effect of roughness in the estimation of the skin friction. For that reason, only the simulated smooth disk is plotted to compare.

It would be have been interesting to really extract relevant data from the hot film anemometer and a careful analysis of the conditions of the water needs to be done before any hot film measurement is carried out.

On the other hand, the use of an experimental technique that allow the collection of data through the boundary layer to compare also turbulence statistics such as RMS and perhaps vorticity would be also desirable. Due to time issues, this part of the validation was not possible to explore, but it might be something to keep an eye on for future work.

6 Chapter VI: Conclusions

After analyzing and comparing the results calculated through CFD and the measurements obtained with the experiments, there are two main conclusions.

The first one is about the use of a rotating disk as an approximation of the flat plate. Although little differences have been seen between the *smooth flat plate* and the *smooth rotating disk*, the behavior of the flow for both cases with the roughness have a very high match. It is known that the effect of roughness on the inner layer of the boundary layer is important, and the velocity profiles show that the effect is similar when compared flat plate and rotating disk. Although one of the graphs show some differences in turbulent parameters like Reynolds stresses, we mainly observed that the effect is almost the same for the rotating disk and flat plate cases without and with roughness. This adds to the controversy of whether the turbulent structures of flow over rough surfaces are affected by the presence of these rough elements. In light of the results from this study, the approximation between flat plate and rotating disk is believed to be valid and both cases can be compared.

The second conclusion is about the validity of the CFD simulations that have been carried out. Only two parameters have been studied in the experiments due to the limitation of time of this project and also the limitation of data measured with the *hot-film anemometry*. Although the evolution of the parameters measured with the Reynolds number is similar on both cases (experimental and CFD), more comparisons need to be made in order to fully validate the accuracy of the simulations that have been made. However, the behavior of results from the experimental study initially agrees with the results obtained with the CFD.

Additionally, a few studies have been recommended as further work after this project, which are believed to give important information in the validation of the use of a rotating disk as an approximation of a flat plate when the study is focused on the boundary layers.

6.1 Further work

Here there is a list of what is believed to give important information and data for further experiments and simulations:

- Studying the transition: the effect of roughness on the transition is considerable and it should be studied in order to fully understand the development of the boundary layer over a rotating disk. A study of the transition on a disk in the radial direction is recommended.

- Simulations with different CFD models: the model used in this project is believed to give very good results. However, it is recommended to also use a different CFD model and compare the results with the aim of validating the results.

- Set up different boundary conditions: in the rotating disk case, changing the boundary conditions of the *intern* and *extern* surfaces to a *periodic*

transformation (the same used between the *inlet* and *outlet* surfaces) may give more accurate results. A simulation changing the boundary conditions is recommended.

- Changing the geometry: this recommendation is only applied to the rotating disk. Instead of the geometry studied on this project, a portion of the disk (from the center to the edge) or the full disk can be simulated.

    - Note: an *O-grid* is needed in order to avoid mesh problems at the center of the disk.

- Pre-warm up the water before collecting the data: as explained in the 5.4 section, the data might not be reliable due to the non-optimal conditions of the water inside the tank. Therefore, ensuring that the water does not contain contaminants and proper warm up procedures to avoid large temperature variations in the water are recommended, especially during seasons like summer, when the ambient temperatures can vary substantially.

- Experiment with different measuring techniques: it has been explained that only a few data have been measured using the hot-film anemometry (near the wall values). In order to give more validity to the results, data from all the boundary layer is needed so it can be compared with CFD results. For that reason, it is recommended to measure the experimental values with techniques that do not have the near-the-wall limitation that the hot-film anemometry has.

7 References

[1] d'Alembert, Jean le Rond, "Essai d'une nouvelle theorie de la résistance des fluides", Paris 1752.

[2] Velocity distribution between two flat plates, Thermal-FluidsCentral, accessed 23 September 2015, <https://www.thermalfluidscentral.org/encyclopedia/index.php/Introduction_to_Momentum_Transfer>.

[3] Chklovski, T., "Pointer-tip wings at low Reynolds numbers", accessed 12 September 2015, <http://www.wfis.uni.lodz.pl/edu/Proposal.htm>.

[4] Velocity profile over a flat plate, Convection Heat Coefficient, SolidWorks help 1995-2015, accessed 28 August 2015,

<http://help.solidworks.com/2014/English/SolidWorks/cworks/c_convection_heat_coefficient.htm?format=P>.

[5] Wereley, S. T.; Lueptow, R. M. (1999). "Velocity field for Taylor–Couette flow with an axial flow". Physics of Fluids 11 (12): 3637–3649.

[6] Simple Couette configuration using two infinite flat plates, Couette flow, accessed 12 September 2015, <https://en.wikipedia.org/wiki/Couette_flow>.

[7] P. Ram and K. Sharma, "Revolving Ferrofluid Flow under the Influence of MFD Viscosity and Porosity with Rotating Disk," Journal of Electromagnetic Analysis and Applications, Vol. 3 No. 9, 2011, pp. 378-386.

[8] Crowe, C., Elger, D. and Roberson, J. (2005): "Engineering Fluid Mechanics", Wiley, Eighth Edition.

[9] Visavale, Ganesh (2014), "Y+ Wall Function in CFD", accessed 20 August 2015,

<https://www.linkedin.com/pulse/20140725081243-58050580-y-wall-function-in-cfd>.

[10] von Kármán, Th. (1930), "Mechanische Ähnlichkeit und Turbulenz", Nachrichten von der Gesellschaft der Wissenschaften zu Göttingen, Fachgruppe 1 (Mathematik) 5: 58–76 (also as: "Mechanical Similitude and Turbulence", Tech. Mem. NACA, no. 611, 1931).

[11] Germano, M., Piomelli, U., Moin, P. and Cabot, W. H. (1991), "A dynamic sub-grid scale eddy viscosity model", Physics of Fluids, A(3): pp 1760-1765, 1991.

[12] Reynolds, Osborne, 1895: "On the Dynamical Theory of Incompressible Viscous Fluids and the Determination of the Criterion." Philosophical Transactions of the Royal Society of London. A, v. 186, pp. 123-164.

[12] Linear eddy viscosity models. (2011, June 7). Retrieved September 16, 2015, from <http://www.cfd-online.com/Wiki/Linear_eddy_viscosity_models>.

[13] Henk Kaarle Versteeg, Weeratunge Malalasekera (2007). An Introduction to Computational Fluid Dynamics: The Finite Volume Method. Pearson Education Limited.

[14] Wilcox, D.C. (1988), "Re-assessment of the scale-determining equation for advanced turbulence models", AIAA Journal, vol. 26, no. 11, pp. 1299-1310.

[15] Menter, F. R. (1993), "Zonal Two Equation k-ω Turbulence Models for Aerodynamic Flows", AIAA Paper 93-2906.

[16] Menter, F. R. (1994), "Two-Equation Eddy-Viscosity Turbulence Models for Engineering Applications", AIAA Journal, vol. 32, no 8. pp. 1598-1605.

[17] Antonia RA, Luxton RE (1971) “The response of a turbulent boundary layer to a step change in surface roughness. Part 1. Smooth to rough”. J Fluid Mech 48(part 4):721–761.

[18] Pavlenko, A. et. Al: ““Hydrodynamics of a Rotating Disk”, report. Department of Applied Mechanics, Division of Fluid Dyncamics, Chalmers University of Technology, Gothenburg, 2015.

[19] Bruun, H.H, (1995): “Hot-Wire Anemometry: Principles and Signal Analysis” Oxford University Press

[20] International Towing Tank Conference (2002), “Resistance Uncertainty Analisys, Example for Resistance Test”, ITTC-Recommended Procedures 7.5-02-02-02, Revision 01, pag 11.

Appendix

The drawings needed for the creation and design of the tank and shaft where the experiments have been carried out are found here. The software used for both the design and the drawings is the SolidWorks 2014. Starting with the shaft:

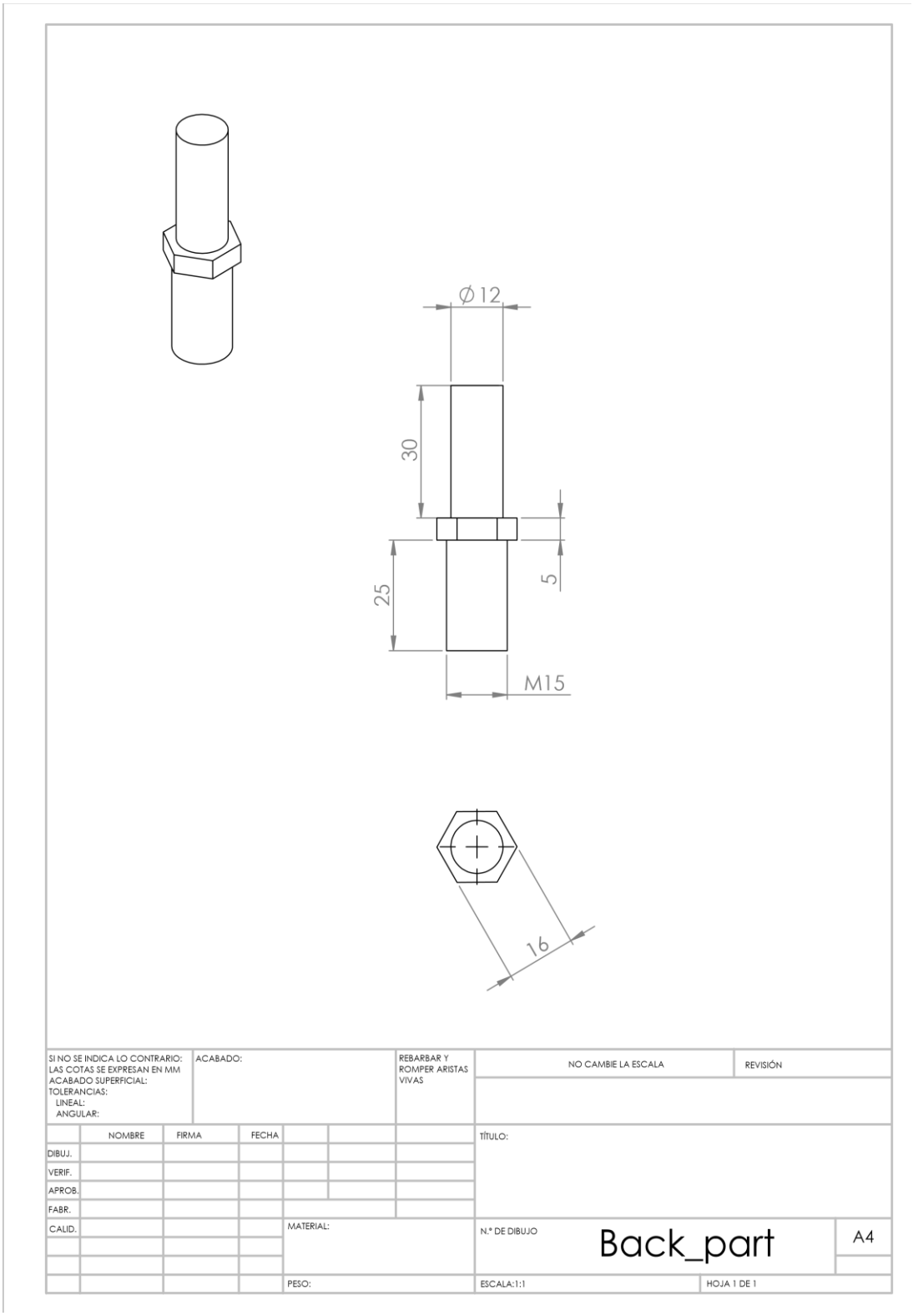

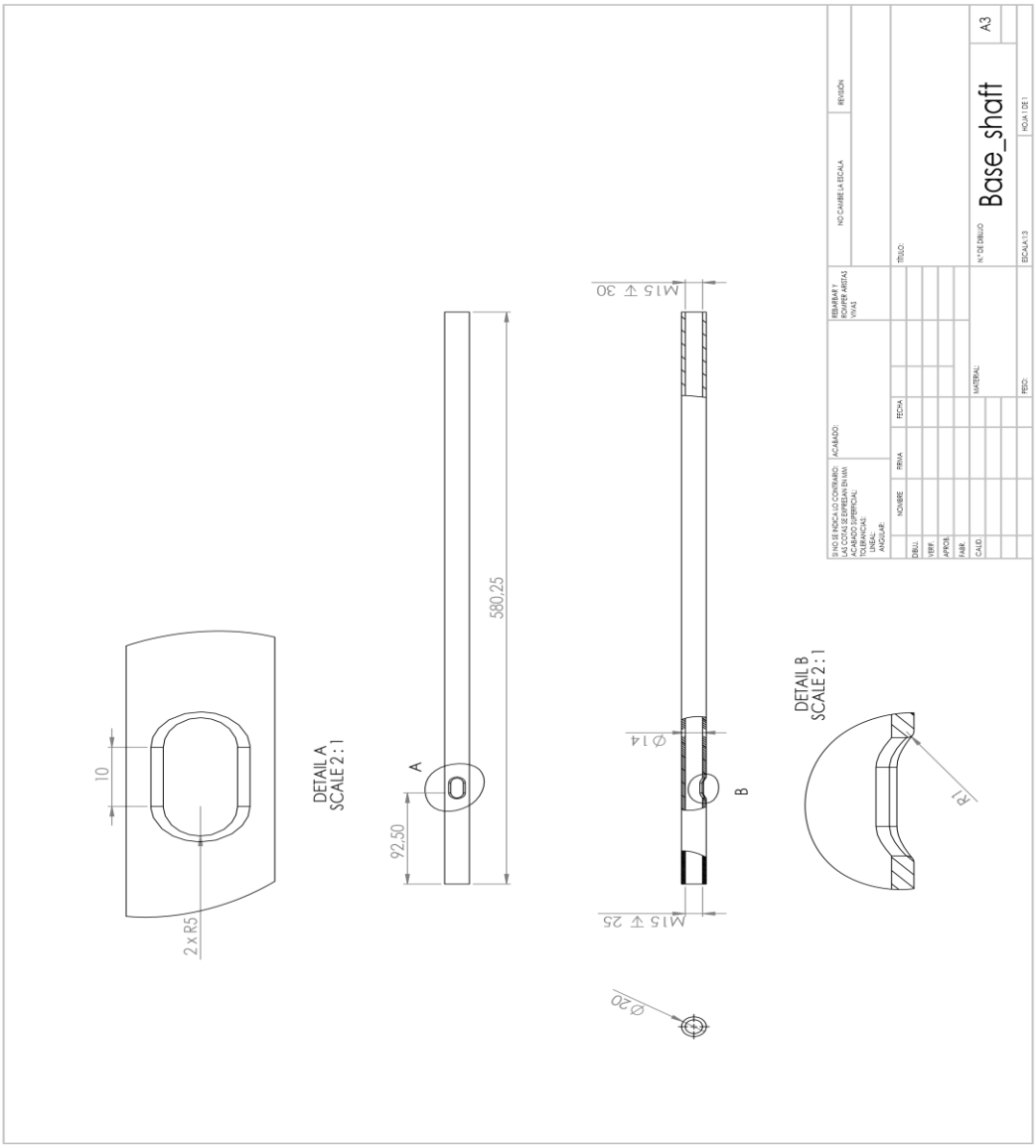
Base_shaft
A3
DETAIL A
SCALE 2 : 1
DETAIL B
SCALE 2 : 1
10
2 x R5
580,25
92,50
A
B
M15 ↧ 30
M15 ↧ 25
Ø 14
Ø 20
R1

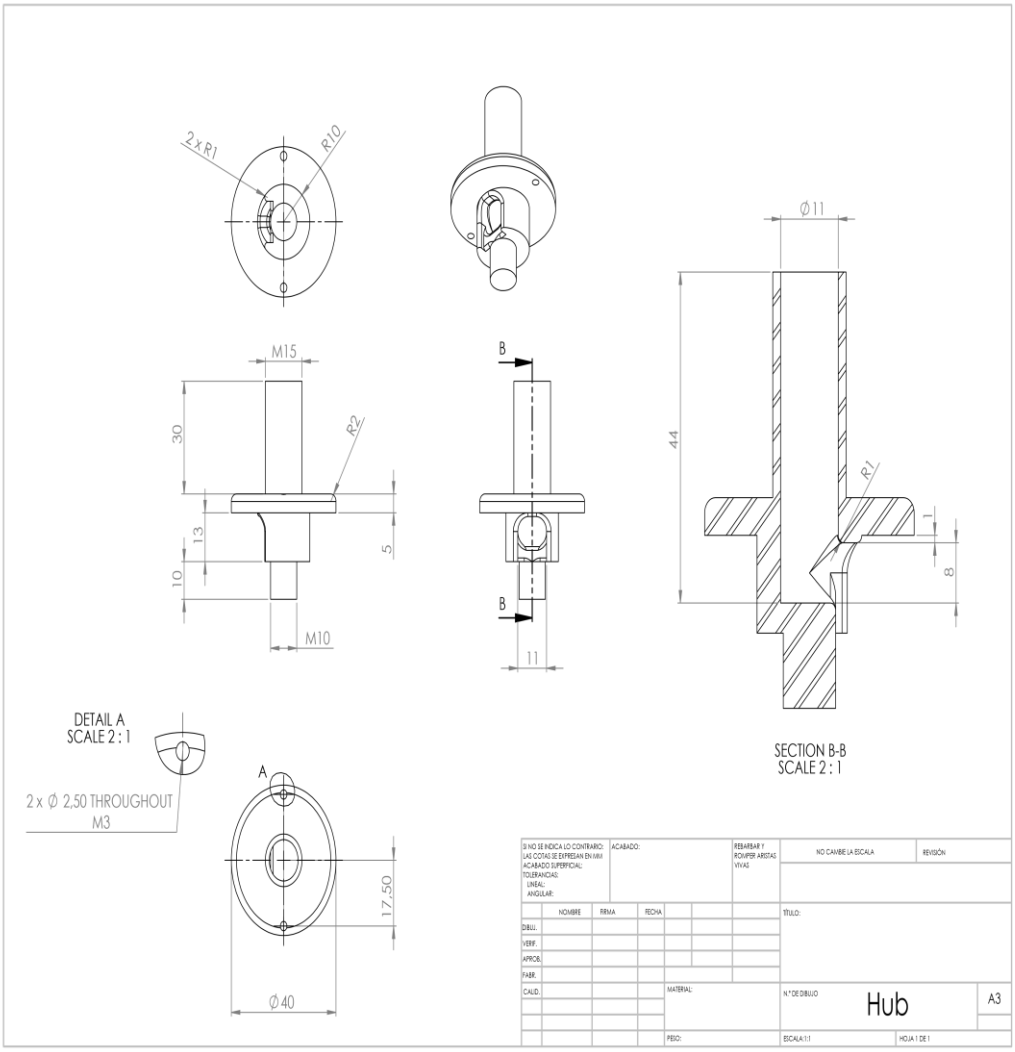
2xR1
R10
M15
30
R2
13
10
5
M10
B
B
11
Ø11
44
R1
1
8
SECTION B-B
SCALE 2 : 1
DETAIL A
SCALE 2 : 1
2 x Ø 2,50 THROUGHOUT
M3
A
17,50
Ø40
Hub
A3

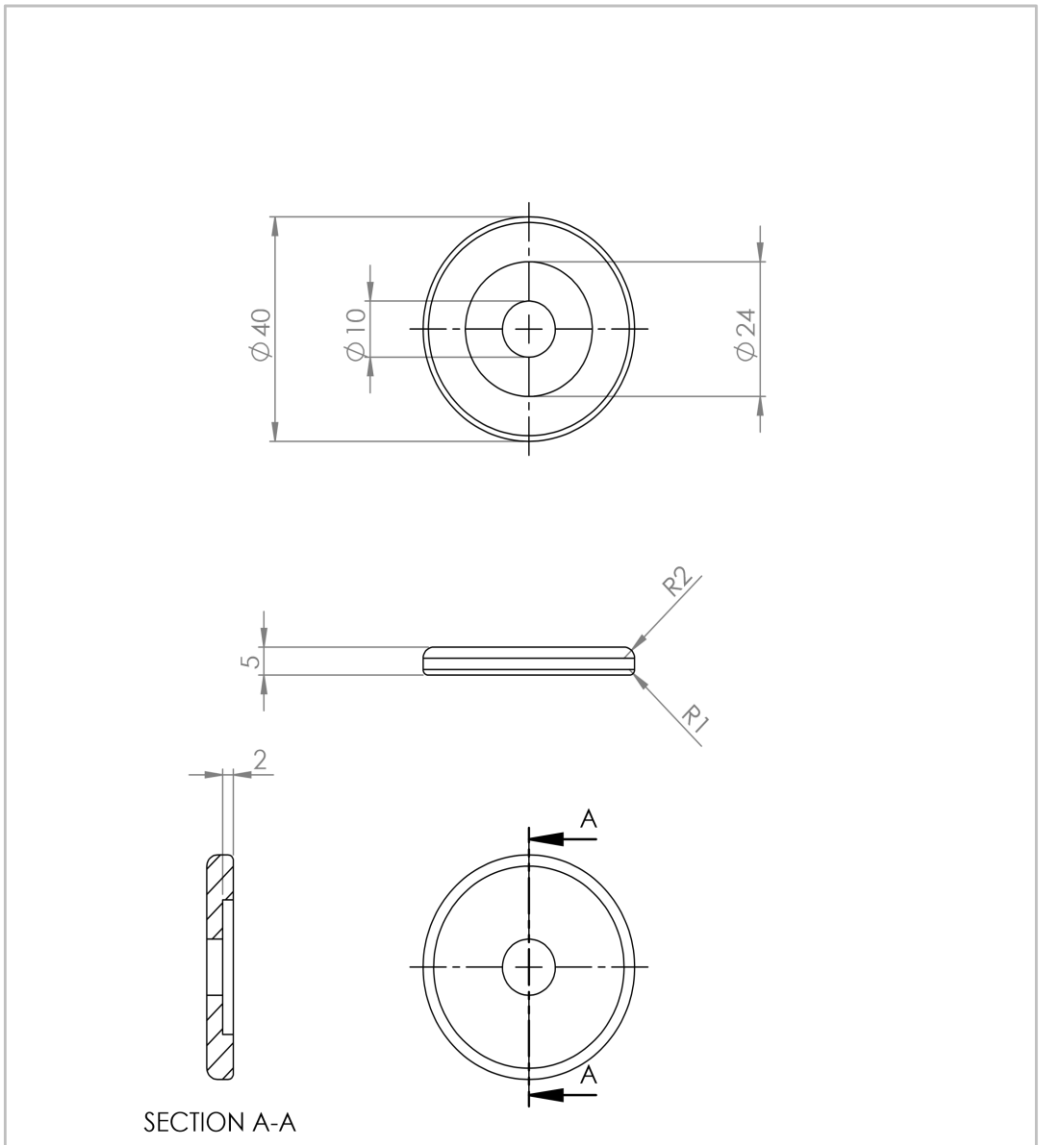

SI NO SE INDICA LO CONTRARIO: LAS COTAS SE EXPRESAN EN MM ACABADO SUPERFICIAL: TOLERANCIAS: LINEAL: ANGULAR:		ACABADO:			REBARBAR Y ROMPER ARISTAS VIVAS		NO CAMBIE LA ESCALA	REVISIÓN
	NOMBRE	FIRMA	FECHA				TÍTULO:	
DIBUJ.								
VERIF.								
APROB.								
FABR.								
CALID.				MATERIAL:			N.º DE DIBUJO	A4
							Front Hub	
				PESO:			ESCALA:1:1	HOJA 1 DE 1

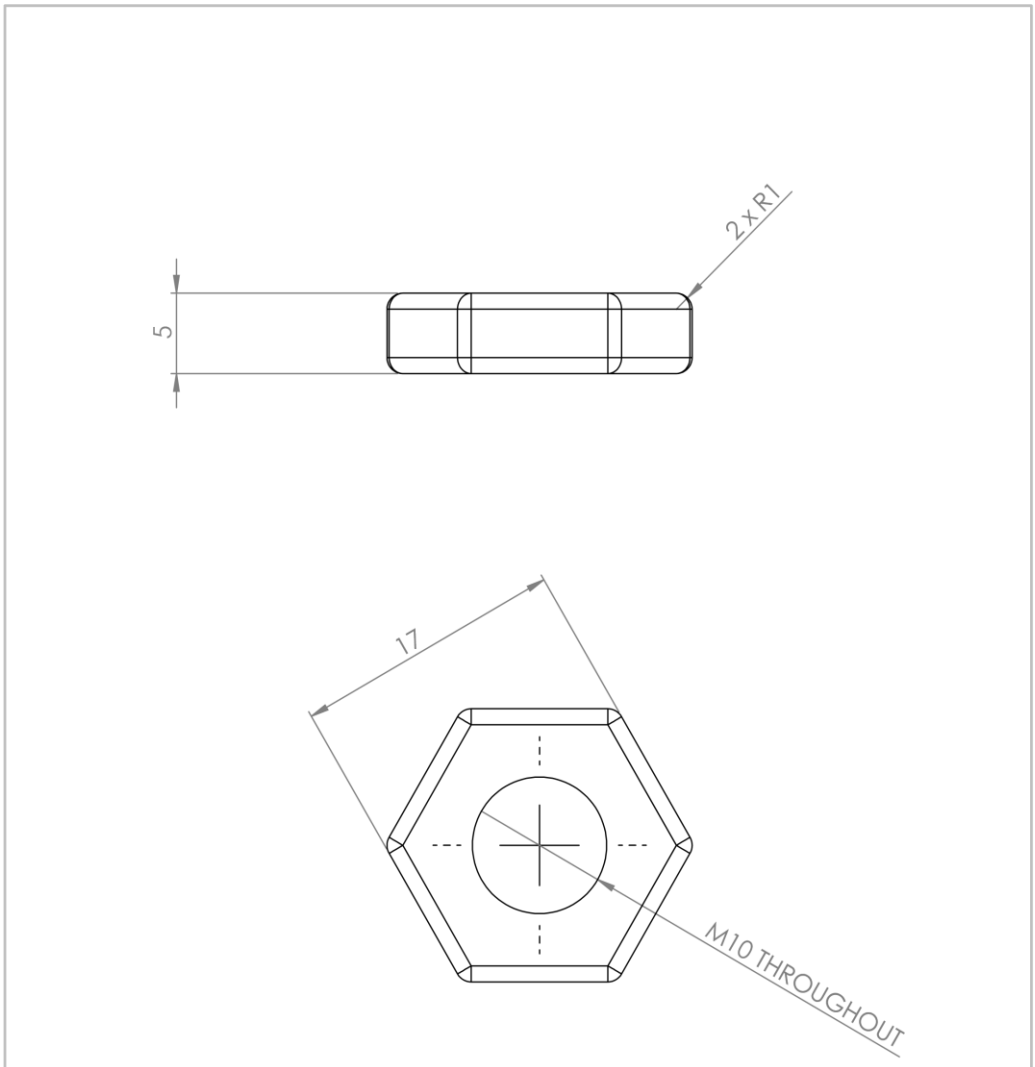

SI NO SE INDICA LO CONTRARIO: LAS COTAS SE EXPRESAN EN MM ACABADO SUPERFICIAL: TOLERANCIAS: LINEAL: ANGULAR:		ACABADO:			REBARBAR Y ROMPER ARISTAS VIVAS	NO CAMBIE LA ESCALA		REVISIÓN
	NOMBRE	FIRMA	FECHA			TÍTULO:		
DIBUJ.								
VERIF.								
APROB.								
FABR.								
CALID.				MATERIAL:		N.º DE DIBUJO	Nut	A4
				PESO:		ESCALA:3:1	HOJA 1 DE 1	

The drawings of the tank are the ones shown below:

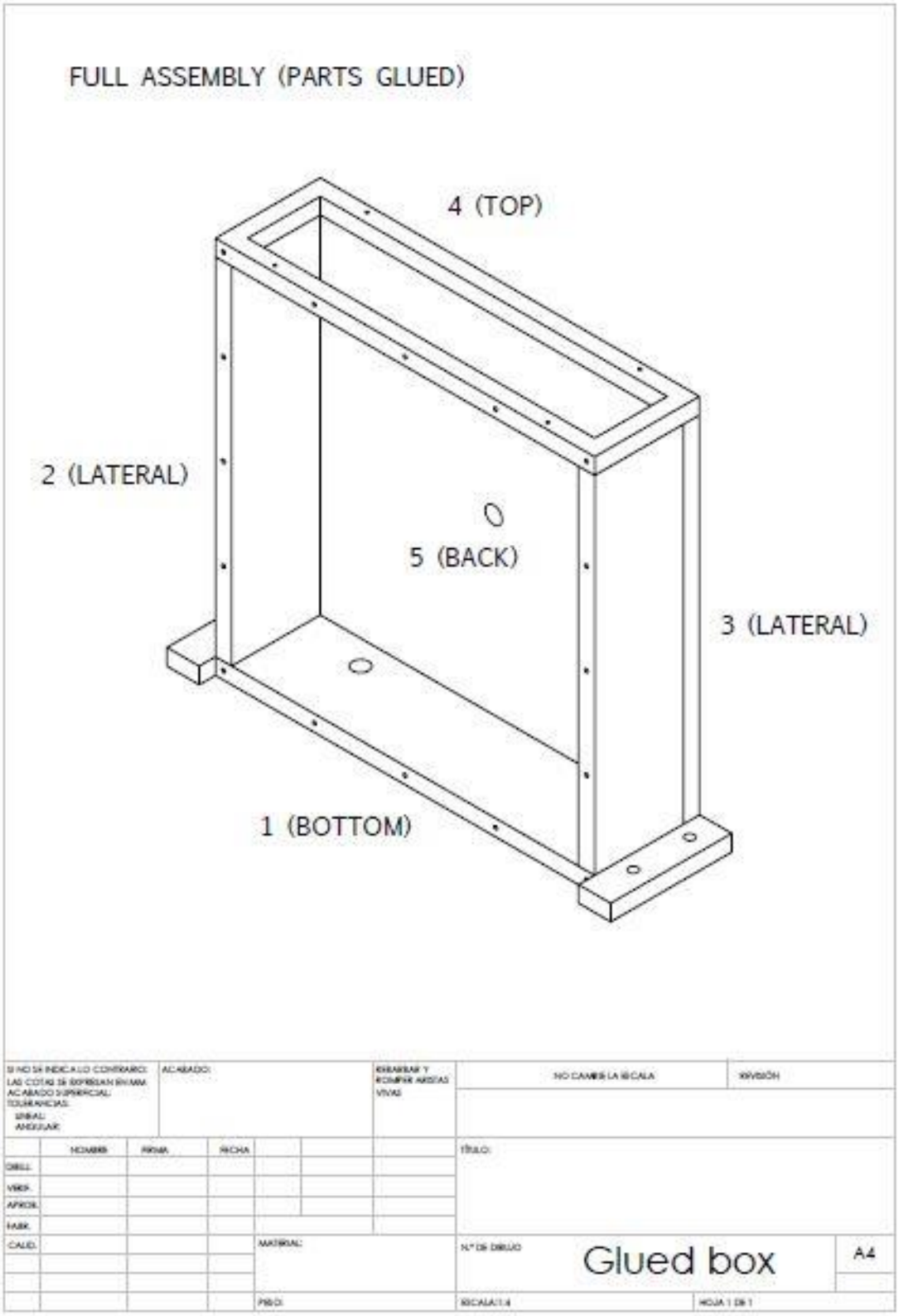

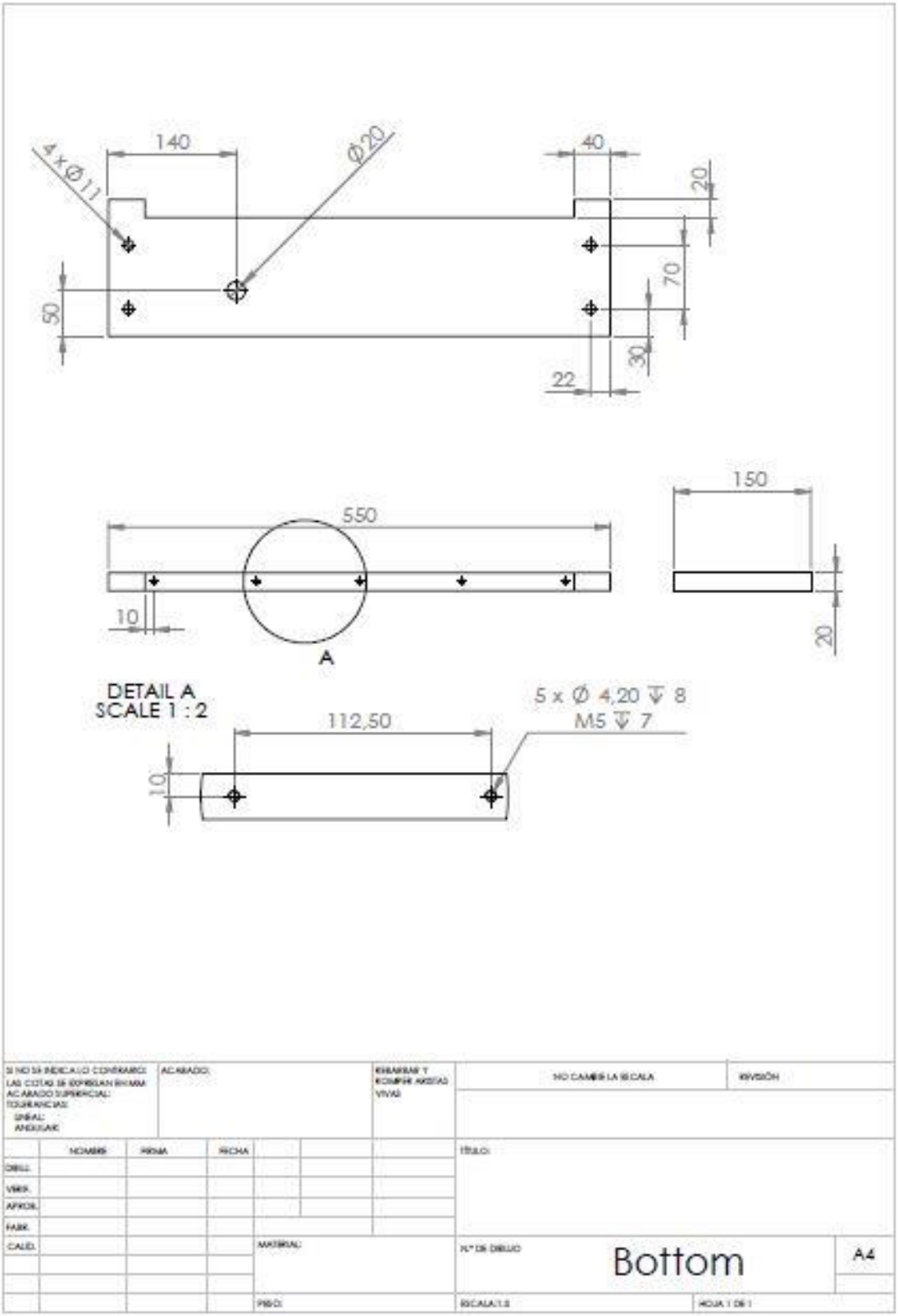
4xØ11
140
Ø20
40
20
70
50
30
22
150
550
10
20
A
DETAIL A
SCALE 1 : 2
5 x Ø 4,20 ↧ 8
M5 ↧ 7
112,50
10
Bottom
A4

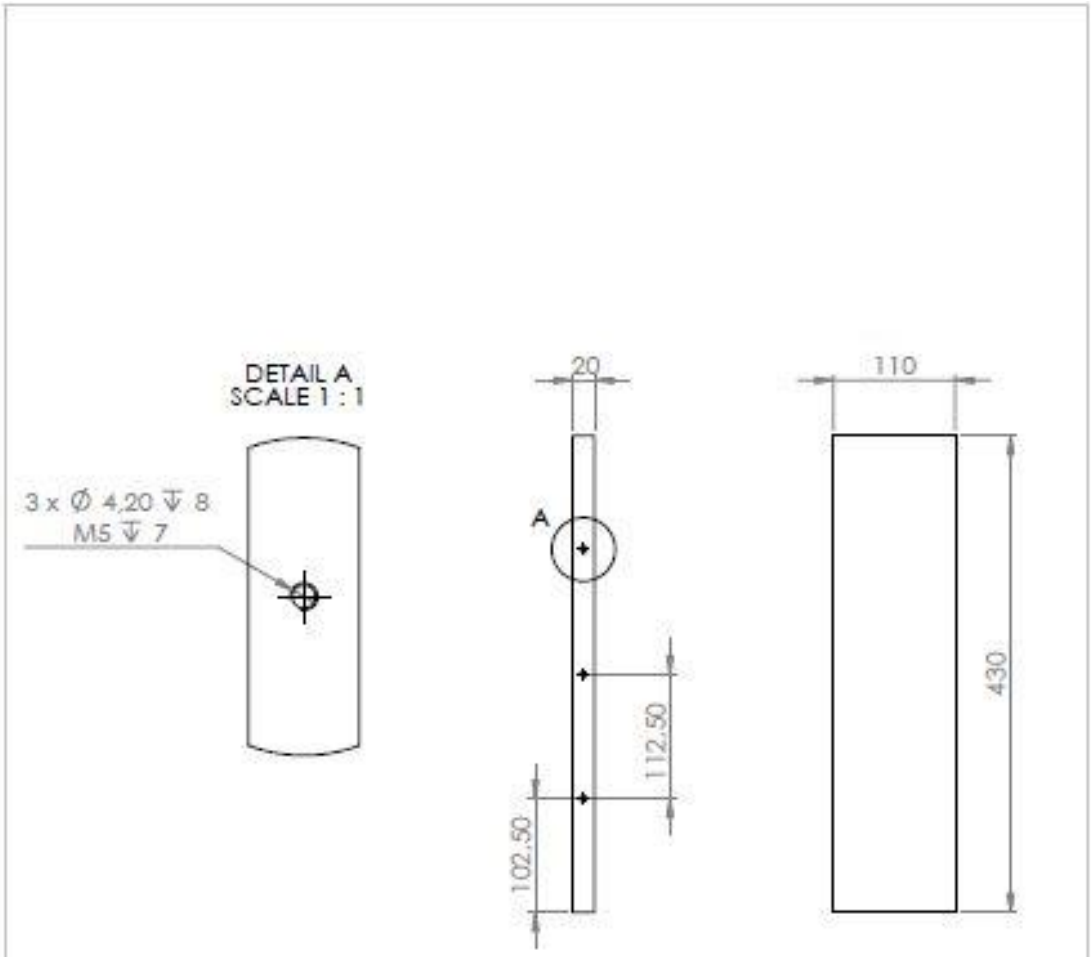

SI NO SE INDICA LO CONTRARIO: LAS COTAS SE EXPRESAN EN MM. ACABADO SUPERFICIAL: TOLERANCIAS: LINEAL: ANGULAR:	ACABADO:			ESMERILAR Y ROMPER ARISTAS VIVAS	NO CAMBIE LA ESCALA		REVISIÓN
	NOMBRE	FIRMA	FECHA				TÍTULO:
DIBUJ.							
VISTO							
APROB.							
FABR.							
CALID.				MATERIAL:			Nº DE DIBUJO: Lateral A4
				PESO:	ESCALA:1:1		HOJA 1 DE 1

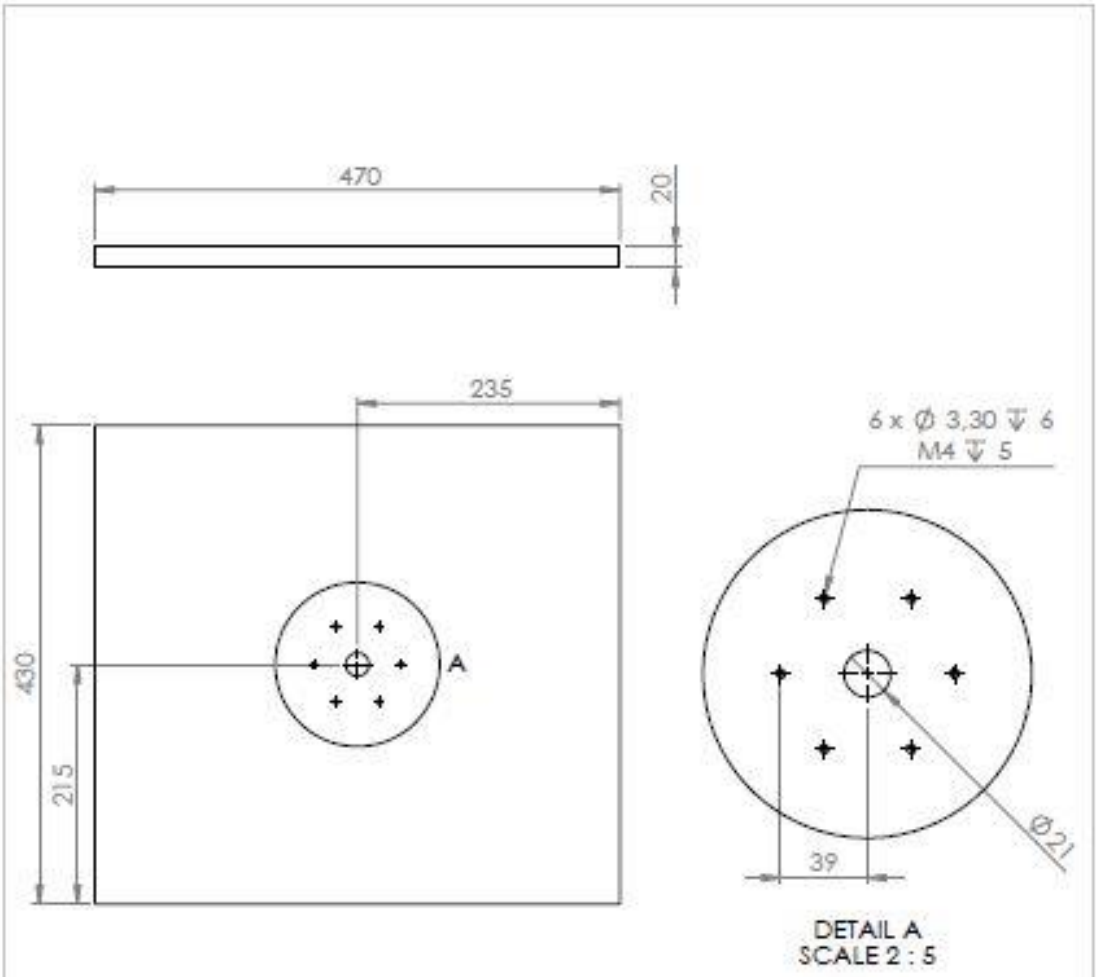

SI NO SE INDICA LO CONTRARIO: LAS COTAS SE EXPRESAN EN MM. ACABADO SUPERFICIAL: TOLERANCIAS: LINEAL: ANGULAR:	ACABADO:				ROMPER ARISTAS VIVAS	NO CAMBIE LA ESCALA	REVISIÓN	
	NOMBRE	FIRMA	FECHA				TÍTULO:	
DIBUJ.								
VISTO.								
APROB.								
FABR.								
CALID.				MATERIAL:			Nº DE DIBUJO	A4
							Back	
				PESO:			ESCALA 1:2	HOJA 1 DE 1

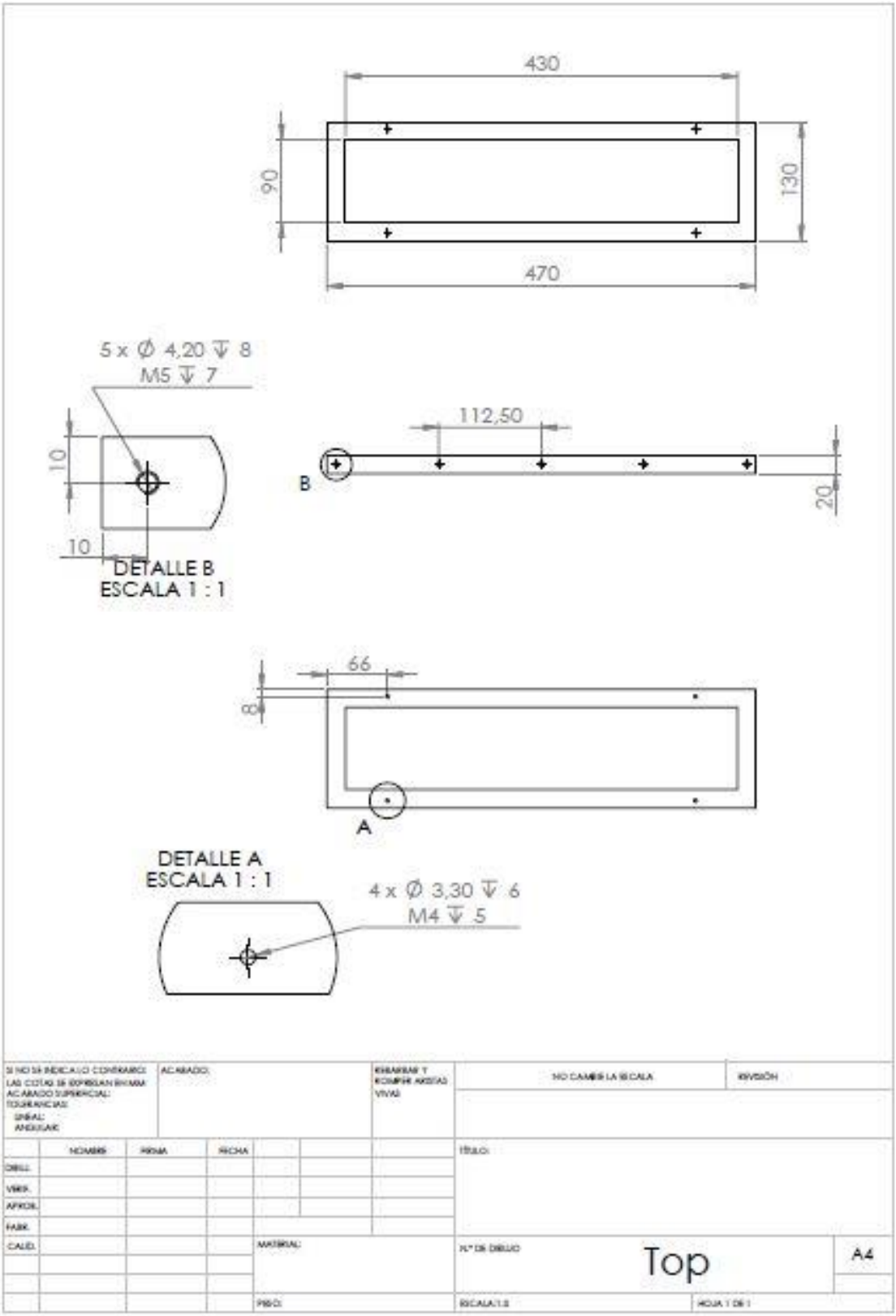
430
90
130
470
5 x Ø 4,20 ↧ 8
M5 ↧ 7
10
10
DETALLE B
ESCALA 1 : 1
112,50
B
20
66
8
A
DETALLE A
ESCALA 1 : 1
4 x Ø 3,30 ↧ 6
M4 ↧ 5
Top
A4

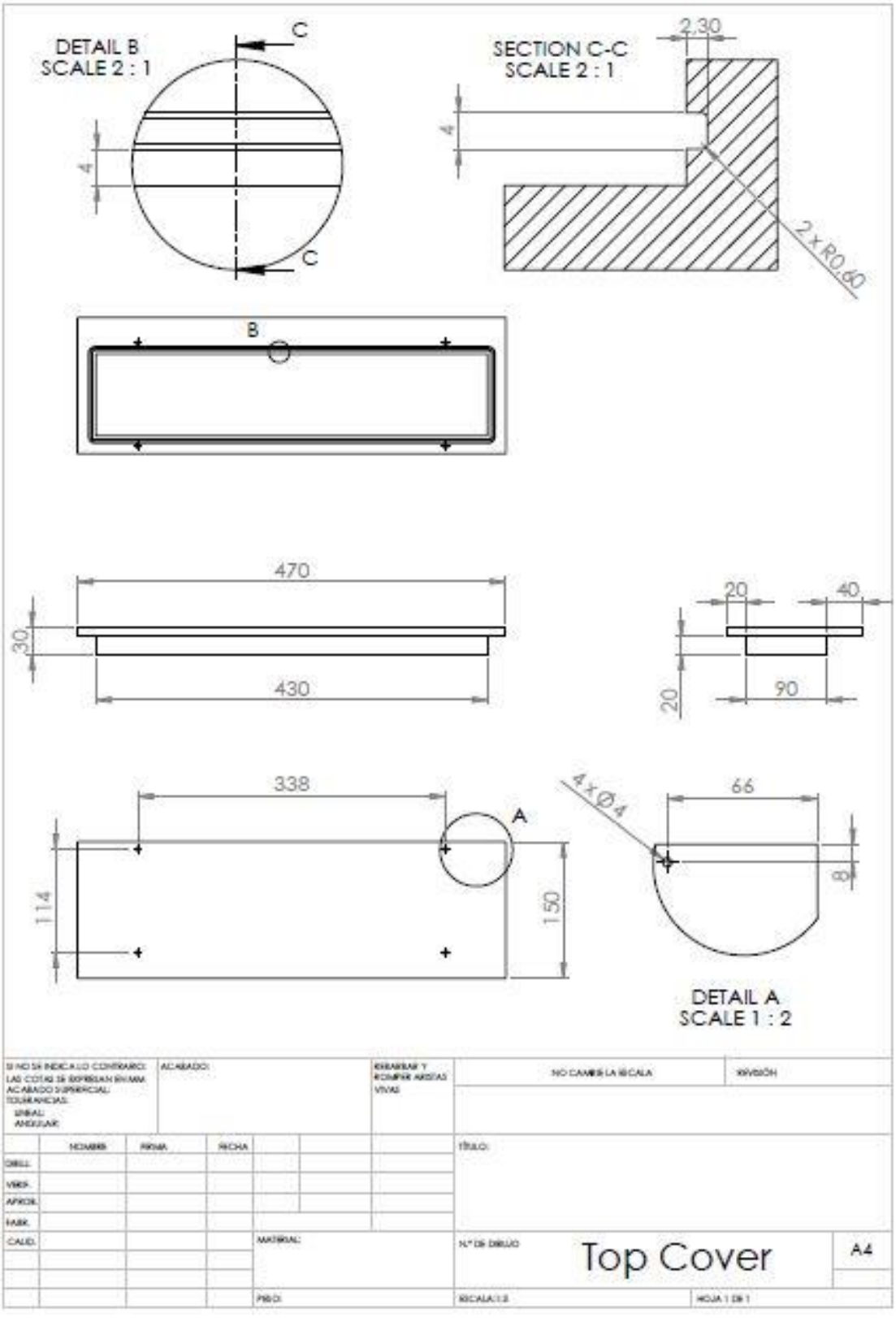
DETAIL B
SCALE 2 : 1
C
C
4
SECTION C-C
SCALE 2 : 1
2,30
4
2 x R0,60
B
470
30
430
20
40
20
90
338
A
114
150
4 x Ø4
66
8
DETAIL A
SCALE 1 : 2
Top Cover
A4

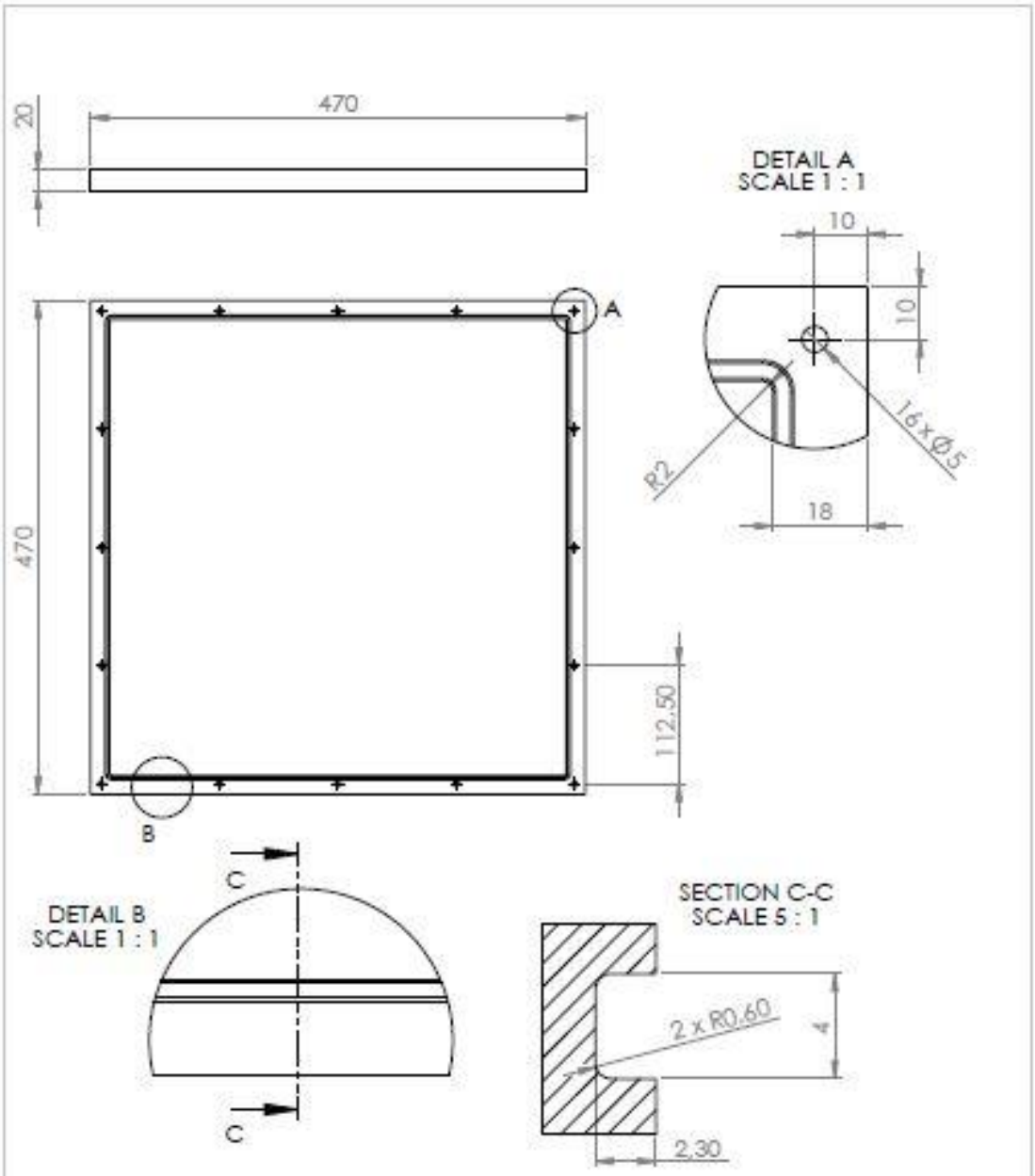
20
470
DETAIL A
SCALE 1 : 1
10
10
16xØ5
R2
18
A
470
112,50
B
C
DETAIL B
SCALE 1 : 1
C
SECTION C-C
SCALE 5 : 1
2 x R0,60
4
2,30
Cover
A4